Aalto University

School of Electrical Engineering
Department of Signal Processing and Acoustics

Timo Dönsberg

Improved Reference Infrared Spectrometer

Thesis submitted for examination for the degree of Master of Science in Technology.

Espoo, 27th of January, 2012

Supervisor: Prof. Erkki Ikonen

Instructor: Dr. Farshid Manoocheri

AALTO UNIVERSITY
SCHOOL OF ELECTRICAL ENGINEERING

ABSTRACT OF THE
MASTER'S THESIS

Aalto University

School of Electrical Engineering

Department of Signal Processing and Acoustics

Author: Timo Dönsberg

Title: Improved Reference Infrared Spectrometer

Date: 27.1.2012 Number of pages: 8+90

Supervisor: Prof. Erkki Ikonen

Instructor: Dr. Farshid Manoocheri

Language: English

Infrared radiation is electromagnetic radiation with a spectrum ranging from 750 nm to 1 mm in wavelength. It is invisible to the human eye, but has significance in optical spectroscopy. An optical spectrometer is a device that measures the emission, absorption, or fluorescence spectrum of a material.

In this work, a reference infrared spectrometer facility at the Metrology Research Institute was upgraded. The spectrometer can be used to measure spectral responsivity of detectors, spectral transmittance of optical materials and spectral power distribution measurements of light sources in the wavelength range of 750 nm to 16 µm. The measurement setup was improved for full automation using LabVIEW and the previous calibration and automation procedures were refined. Automated facility is versatile for different measurement setups and is easy to operate.

Phase sensitive detection is utilized in the measurement setup by using a lock-in amplifier. It enables the detection of very small signals in the presence of overwhelming noise. Optical chopping is used to modulate the measurement signal at a known reference frequency. Typically the linearity of the measurement system is determined optically. Also in this work, a fully electronic method for linearity measurements of lock-in amplifiers was developed and tested. This method improves the accuracy in lock-in comparison measurements.

In addition, a preamplifier for photoconductive detectors was constructed and characterized. The amplifier was designed so that it can be used with wide variety of detectors.

Keywords: infrared, spectrometer, automation, linearity, photoconductive detector

Aalto-yliopisto

Sähkötekniikan korkeakoulu

Signaalinkäsittelyn ja akustiikan laitos

Tekijä: Timo Dönsberg

Työn nimi: Uudistettu referenssi-infrapunaspektrometri

Päiväys: 27.1.2012 Sivumäärä: 8+90

Työn valvoja: Prof. Erkki Ikonen

Työn ohjaaja: TkT Farshid Manoocheri

Kieli: Englanti

Infrapunasäteily on sähkömagneettista säteilyä, jonka aallonpituus on 750 nn – 1 mm. Se on tärkeä työväline optisessa spektroskopiassa, vaikka onkin ihmissilmälle näkymätöntä. Optisella spektrometrillä tarkoitetaan laitetta, joka mittaa materiaalin emissio-, absorptio- tai fluoresenssispektriä.

Tässä työssä uudistettiin Aalto-yliopiston Mittaustekniikan ryhmän referenssi-infrapunaspektrometriä. Laitetta käytetään ilmaisimen vasteen, aineen läpäisyn ja lähteen tehojakauman spektrisiin mittauksiin aallonpituusalueella 750 nm – 16 µm. Mittauslaitteisto automatisoitiin käyttäen LabVIEW-ohjelmistoa. Lisäksi kalibrointi- ja mittausmenetelmiä paranneltiin. Automatisoitu mittauslaitteisto soveltuu monipuolisesti erilaisiin mittausjärjestelyihin ja on aiempaa helpompi käyttää.

Mittauksissa käytetään vaihelukittua vahvistinta, joka mahdollistaa hyvin heikkojen signaalien havaitsemisen suuren kohinasignaalin läsnäolosta huolimatta. Mitattavaa signaalia moduloidaan katkomalla valolähdettä referenssitaajuudella. Optisen menetelmän sijaan vaihelukitun vahvistimen lineaarisuusmittauksiin kehitettiin täysin sähköinen menetelmä, joka parantaa ulkoista tarkkuutta vertailumittauksissa.

Lisäksi osana työtä suunniteltiin, rakennettiin ja karakterisoitiin esivahvistin valojohtaville ilmaisimille. Tavanomaisesta sovitetusta esivahvistimesta poiketen laitteen keskeiset parametrit ovat säädettäviä, joten sitä voidaan käyttää lukuisien eri ilmaisimien kanssa.

Avainsanat: infrapuna, spektrometri, automaatio, lineaarisuus, valojohtava ilmaisin

Acknowledgements

This work has been done at the Metrology Research Institute (MRI) of the Aalto University School of Electrical Engineering. The research project was funded by the Centre for Metrology and Accreditation (MIKES).

I would like to thank Professor Erkki Ikonen, the head of the Metrology Research Institute, for supervising this work, and for giving me the opportunity and encouragement to work on many challenging and interesting projects.

I am most grateful for my instructor Dr. Farshid Manoocheri for the support, comments and advices that helped me to overcome all the obstacles on the way. After countless constructive and instructive conversations I can only admire his wisdom to always ask the right questions and, moreover, his patience to listen to my answers.

It is a pleasure and a privilege to work among the personnel of the Metrology Research Institute. The both relaxed and productive working atmosphere is something truly unique, of which I want to thank all my co-workers.

I am deeply thankful to my parents, who have always given me love, understanding, support, and the freedom to make my own decisions, and to my sister, who still keeps guiding her little brother in life. I also want to thank all my friends, who have given me aid, trust, joy and a change to follow my many passions in life.

Finally, I wish to thank my dear girlfriend Julia for making my life the one I want to live.

Espoo, 23th of January, 2012

Timo Dönsberg

Table of Contents

Symbols and Abbreviations

A_d	Active area of a detector	
A_e	Electrical area of a detector	
A_m	Amplitude of a measurand signal	
A_o	Optical area of a detector	
A_r	Amplitude of a reference signal	
A_s	Source area	
AC	Alternating Current	
ADC	Analog-to-Digital Converter	
APD	Avalanche Photodiode	
b	Wien's displacement constant	$\approx 2{,}8977685 \cdot 10^{-3}$ m·K [1]
b_c	Maximum contrast constant	$\approx 2{,}410 \cdot 10^{-3}$ m·K [2]
B	Optical band pass	
B_n	Noise equivalent bandwidth of measurement system	
BNC	Bayonet Nut Coupling	
c	Speed of light	
C	Capacitance	
c_0	Speed of light in vacuum	$= 299\,792\,458$ m·s^{-1} [1]
CSV	Comma-Separated Values	
d	Grating constant	
D	Detectivity	
D^*	Specific detectivity	
DC	Direct Current	
DLL	Dynamic Link Libraries	
E_e	Irradiance	
$E_{e\lambda}$	Spectral irradiance	
E_g	Band gap energy	
E_p	Energy of a photon	
f_c	Cut-off frequency	
ECPR	Electrically Calibrated Pyroelectric Radiometer	
EEPROM	Electronically Erasable Programmable Read-Only Memory	
FPA	Focal-Plane Array	
G	Gain	
h	Planck constant	$\approx 6{,}626\,069\,57 \cdot 10^{-34}$ J·s [1]
HUT	Helsinki University of Technology	
I_d	Dark current	
I_{det}	Detector current	
I_e	Radiant intensity	
$I_{e\lambda}$	Spectral radiant intensity	
I_{out}	Output current	
IR	Infrared	
JNI	Java Native Interface	
k	Angular wavenumber	
k_B	Boltzmann constant	$\approx 1{,}3806503 \cdot 10^{-23}$ J·K^{-1} [1]

L_e	Radiance
$L_{e\lambda}$	Spectral radiance
LASER	Light Amplification by Stimulated Emission of Radiation
LCD	Liquid Crystal Display
LED	Light Emitting Diode
m	Diffraction order
M_e	Radiant exitance or radiant emittance
MASER	Microwave Amplification by Stimulated Emission of Radiation
MCT	Mercury Cadmium Telluride
N	Number of measurement samples
NEB	Noise Equivalent Bandwidth
NEI	Noise Equivalent Irradiance
NEP	Noise Equivalent Power
NI	National Instruments
P_{inc}	Incident optical power
PCB	Printed Circuit Board
PEM	Photoelectromagnetic
PSD	Phase Sensitive Detector
PPTC	Polymeric positive temperature coefficient
Q_e	Radiant energy
QDIP	Quantum Dot Infrared Photodetector
QWIP	Quantum Well Infrared Photodetector
R	Magnitude
R_1	Resistance in amplifier model
R_2	Resistance in amplifier model
R_a	Attenuator resistance to input
$R_{a\|\|b}$	Parallel connection of R_a and R_b
R_b	Attenuator resistance to ground
R_D	Dark resistance
R_{IN}	Input resistance
R_L	Load resistance
RMS	Root Mean Square
S	Responsivity
SI	International System of Units (French: *Système international d'unités*)
SNR	Signal-to-Noise Ratio
t	Time variable
T	Absolute temperature
T_{ext}	Temperature of an external enclosure
u_m	Measurand signal
u_{in}	Input signal
u_n	Noise component
u_r	Reference signal
$\tilde{u}_r$	Phase shifted reference signal
UV	Ultraviolet
V_{att}	Attenuated voltage
V_B	Bias voltage
V_{in}	Input voltage

V_n	Noise voltage
V_O	Extraction voltage of a photoconductive detector
V_{out}	Output voltage
VAC	Voltage in Alternating Current
VI	Virtual Instrument
VISA	Virtual Instrument Software Architecture
X	Lock-in amplifier X output
w	Width of a monochromator's exit slit
y	Distance from the optical axis
Y	Lock-in amplifier Y output
Z_{in}	Input impedance
Z_{out}	Output impedance
α	Ratio of load resistance and dark resistance
ΔV_O	Output voltage sensitivity
$\Delta V_{O,max}$	Maximum of output voltage sensitivity
$\Delta \Phi_e$	Net radiant flux
ε	Emissivity
η	Load resistance efficiency of photoconductive resistor
θ	Angle between viewpoint and surface normal
θ_d	Diffraction angle
θ_i	Angle of the incident light
λ	Wavelength
λ_0	Photon wavelength in vacuum
λ_c	Cut-off wavelenght
$\lambda_{c,max}$	Wavelength for maximum spectral radiance contrast
λ_m	Wavelength corresponding to diffraction order m
λ_{max}	Wavelength for maximum spectral radiance
Λ	Nominal attenuation
υ	Frequency
$\tilde{\upsilon}$	Wavenumber
ρ_y	Reciprocal linear dispersion
σ	Stefan–Boltzmann constant $= 5{,}670\ 373 \cdot 10^{-8}\ \mathrm{J \cdot s^{-1} \cdot m^{-2} \cdot K^{-4}}$ [1]
φ_m	Phase shift
Φ_e	Radiant flux
$\Phi_{e\lambda}$	Spectral power
ω_r	Reference frequency

1 Introduction

We are constantly surrounded by electromagnetic radiation. Most of it goes unnoticed, since only a small part of the radiation spectrum is visible to human eye. The vast region of optical radiation that has longer wavelength than visible light, yet shorter than microwaves, is known as infrared radiation. A major part of molecular electronic transitions as well as vibrations and rotations in molecules occur in the energy range of an infrared photon. Therefore, infrared radiation offers an interesting research field in the radiometric sciences. Furthermore, common applications of infrared radiation, such as thermal imaging, medical treatment, surveillance or meteorology, affect our everyday lives.

This work continues the infrared radiometry project at the Metrology Research Institute. In the first phase of the project, a facility for spectral responsivity measurements of infrared detectors was established [3]. The facility was then adapted for transmittance measurements and the nitrogen purging was also introduced [4]. The latest major improvement was the extension of the spectral responsivity scale using a pyroelectric reference detector [5]. The versatile measurement facility is currently capable of measuring spectral responsivity, spectral transmittance and spectral power distribution in the wavelength range of 750 nm to 16 µm.

The second chapter outlines the essential theory of infrared radiometry, whereas the improved measurement setup is introduced in the third. The main improvements are related to stable sourcing of infrared radiation and refining the quality of measured electric signal. Also the low frequency response of the pyroelectric reference detector was determined. In addition, all measurement and control devices were mounted to a rack cabinet and the setup was completely automated. The setup automation and measurement procedures are treated in the fourth chapter.

Phase sensitive detection is utilized in the measurements by using a device called a lock-in amplifier. It enables the detection of very small signals in the presence of overwhelming noise. Optical chopping is required to modulate the measured light at a

known reference frequency. However, the accuracy and linearity of lock-in amplifiers are poorly reported and test measurements commonly make use of complicated optical setups. Therefore, development and testing of a purely electrical testing method for the lock-in amplifier was taken as an objective of this thesis. The method and the measurements are introduced in the fifth chapter.

Photoconductive detectors are commonly used in infrared measurements. Different types of detectors have very different properties and are generally used with a matched preamplifier. As a part of the thesis, requirements for a more universal preamplifier were studied, and such a device was then designed, built and characterized. The preamplifier and optical measurement for which it was used are introduced in the sixth chapter.

2 Theory of infrared radiometry

2.1 Fundamentals

The energy of a photon E_p depends only on its frequency υ or inversely, its wavelength λ via the relation

$$E_p = h\nu = \frac{hc}{\lambda}, \tag{2.1}$$

where c is the speed of light and h is the Planck constant ($6{,}626\,069\,57 \cdot 10^{-34}$ J·s or $4{,}136\,667\,516 \cdot 10^{-15}$ eV·s). Therefore the spectrum of electromagnetic radiation can be denoted equivalently in terms of energy, frequency or wavelength [6]. It should be noted that the speed of light and the wavelength of a photon are dependent of the propagation medium and in general, wavelength refers to photon's energy using the speed of light in vacuum c_0 (299 792 458 m·s^{-1}) and the corresponding wavelength λ_0. Often used quantities are also the angular wavenumber k and the spectroscopic wavenumber $\tilde{\upsilon}$ [7]:

$$k = \frac{2\pi}{\lambda},\ \tilde{\upsilon} = \frac{1}{\lambda} = \frac{\nu}{c} = \frac{k}{2\pi}. \tag{2.2}$$

2.1.1 Infrared spectrum

The electromagnetic spectrum with commonly used division to categories is presented in figure 2.1. Wavelengths ranging from 5 nm to 1 mm are traditionally considered to be the region of optical radiometry. Only a tiny fraction of the whole range, wavelengths between 380 nm and 760 nm, are visible light. Slightly different values for both definitions can be found in literature. In any case, optical radiation with shorter wavelength, or correspondingly higher energy, and optical radiation with longer wavelength and lower energy are called ultraviolet (UV) and infrared (IR) radiation, respectively [8].

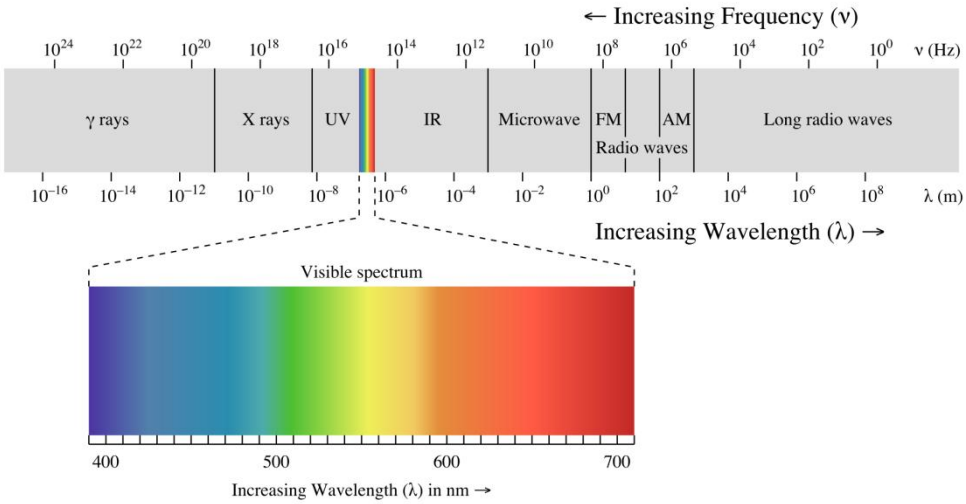

Figure 2.1 The Electromagnetic spectrum. [9]

There are countless standards and conventions based on context and applications for subdividing the vast infrared region. For the purposes of this study, a division commonly used in astronomy was used. This division, also presented in Figure 2.2, was selected mainly for practical reasons, as it was also used in all the previous works [3], [4] and [5]. The infrared spectrum is split into three regions. Near infrared region (NIR) includes wavelengths from the end of the visible spectrum, around 760 nm, up to 5 µm. Mid infrared region (MIR) covers the range between 5 µm and 30 µm. Far infrared region extends all the way to the edge of microwave frequencies, from 30 µm to 1 mm. These regions are also known as short-wave, mid-wave and long-wave infrared regions, respectively. The region overlapping far infrared and microwave radiations is often referred as the terahertz waves. The measurement setup improved as a part of this thesis was originally used mainly in the near infrared region [3], but was later extended to the mid infrared regime, covering wavelengths up to 16 µm [5].

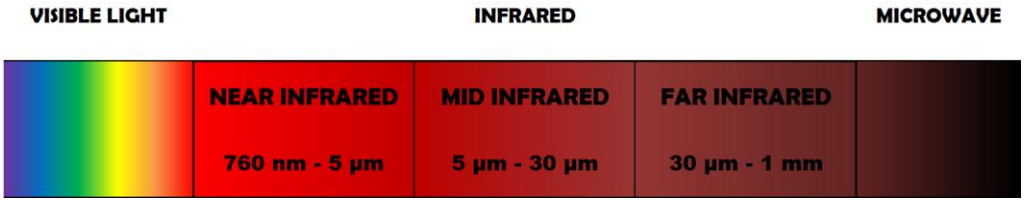

Figure 2.2 One commonly used subdivision for infrared region, also used in the scope of this work.

2.1.2 Spectrometer

Any device that measures any kind of spectrum is a spectrometer, *per se*. In an optical spectrometer, however, the emission, absorption, or fluorescence spectrum of a material is measured. The wavelength selection can be accomplished for example by using optical filters, prisms, gratings, Fourier-transform techniques, tunable lasers, or combinations of the methods mentioned above [10]. The measurement setup concerning this thesis uses optical filters and a monochromator with a single grating in a so called Czerny-Turner mount, both discussed later in chapters 2.4 and 3.3.

2.2 Sources of infrared radiation

In general, any device transforming energy into the optical part of the electromagnetic spectrum is a light source, but for all practical purposes a light source should provide enough constant radiant power in the wavelength region in hand. The emission of an optical source can be either spontaneous or stimulated, and both types of radiation sources are available in infrared region. For the purposes of this work only electrically powered light sources were studied.

In spontaneous emission a transition from an excited energy state to a lower energy state occurs. This can happen in an atom, molecule or nanomaterial that is excited, for instance, by heat, electric arc, electromagnetic radiation or electron-hole pair recombination. Incandescent lamps are based on thermal excitation and have a broad output spectrum. Fluorescent lamps usually use ultraviolet light for excitation of fluorescent material and produce wide spectrum with notable peaks. Gas-discharge

lamps have narrow emission lines, which depend on the gas or gas mixture in question, whereas light emitting diodes typically emit monochromatic light. A broadband spectrum is usually needed in monochromator-based radiometry, but in some cases also monochromatic or narrowband sources can be useful.

Stimulated emission on the other hand involves strong energy pumping that excites atoms or molecules in a lasing media. The excited electron is then stimulated by photon, causing it to drop to a lower energy level. This creates in a new photon with the same energy, phase, polarization and direction as the stimulating photon. When the excited state has more electrons than the lower energy state, the rate of stimulated emission exceeds that of absorption, resulting in optical amplification. Lasers, masers and optical amplifiers use stimulated emission.

The theory of an ideal black body radiation source is very useful in many infrared applications and it is described extensively in the first subchapter. The second subchapter deals with incandescent light sources, which are the most commonly used broadband sources in infrared spectroscopy. Various other light sources are introduced in the third subchapter, main focus being in those of broad spectrum. More information on optical sources in general is widely available, for example in [10], [11] and [12], whereas detailed descriptions of infrared sources can be found for instance in [13], [14] and [15].

2.2.1 Ideal black body

Electromagnetic radiation is emitted from all matter with a temperature above absolute zero. A black body is a theoretical idealization of a physical body that absorbs all incident electromagnetic radiation. Since there is no reflected radiation, the black body radiates incandescently in a continuous spectrum that depends only on the body's temperature. The spectral radiance of an ideal black body, that is, power emitted per unit surface area that falls within a given solid angle as a function of wavelength, is defined by Planck’s law

$$L_{e\lambda} = \frac{2hc^2}{\lambda^5\left(e^{\frac{hc}{\lambda k_B T}} - 1\right)}, \tag{2.3}$$

where k_B is the Boltzmann constant (1,380 650 3 · 10^{-23} J·K^{-1}) and T is the absolute temperature. Spectral radiance of a black body as a function of wavelength in different temperatures is plotted in Figure 2.3. A black body is also a perfect Lambertian radiator, meaning that its radiance is independent of view angle, and therefore its radiant intensity I_e is determined by the Lambert's cosine law

$$I_e(\theta) = I_e(0)\cos(\theta) = L_e A_s \cos(\theta) \tag{2.4}$$

where θ is the angle between the viewpoint and the source surface normal, L_e is the source radiance and A_s is the source area. [2]

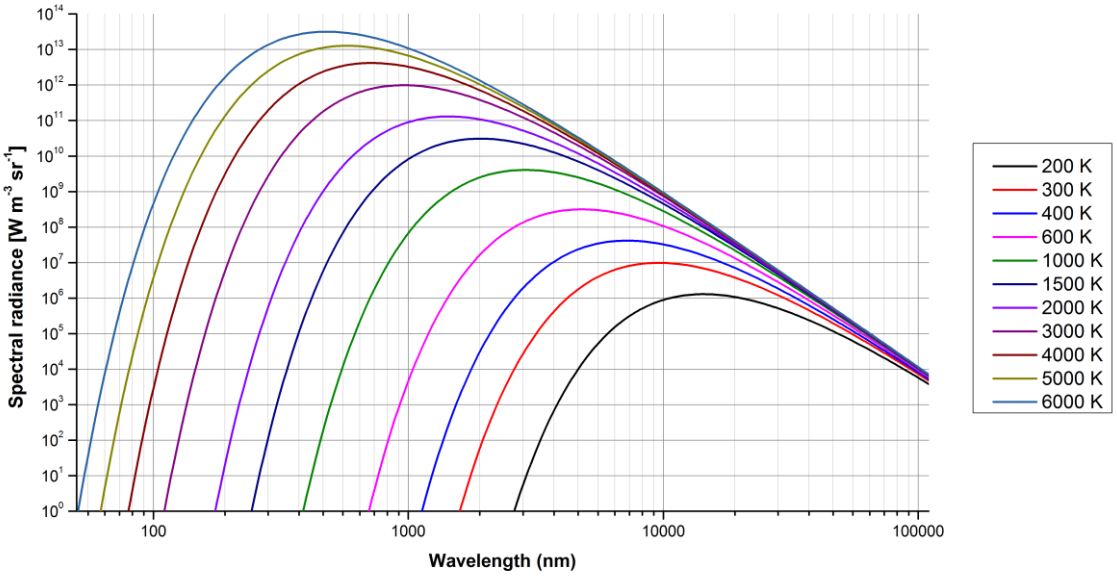

Figure 2.3 Spectral radiance of an ideal blackbody as a function of wavelength in different temperatures.

From figure 2.3 we can distinctly see that the wavelength at which the spectral radiance reaches its maximum decreases when temperature increases. Wavelength for maximum

spectral radiance at a given temperature can be found by setting the partial derivative of equation 2.3 equal to zero

$$\frac{\partial}{\partial \lambda} L_{e\lambda} = 0 \Rightarrow \lambda_{max} = \frac{b}{T}. \tag{2.5}$$

This results is known as Wien's displacement law, where b is called Wien's displacement constant ($2{,}8977685 \cdot 10^{-3}$ m·K). Using this law we can observe, that black or grey bodies having a temperature around 3 – 3800 K will peak of emitted power in the infrared region. Another result somewhat similar to Wien's displacement law is the law for maximum temperature sensitivity of spectral radiance, also known as maximum contrast law. By taking both partial derivatives and the setting the result to zero we can obtain

$$\frac{\partial}{\partial \lambda}\left[\frac{\partial}{\partial T} L_{e\lambda}\right] = 0 \Rightarrow \lambda_{c,max} = \frac{b_c}{T}, \tag{2.6}$$

where b_c is a maximum contrast constant ($2{,}410 \cdot 10^{-3}$ m·K). So, for instance, at a temperature of 300 K the spectral radiance has a maximum around 9,7 µm, but the spectral radiance is most sensitive to temperature changes around 8,0 µm. [2]

The ratio of energy radiated by a physical body to energy radiated by an ideal black body at the same temperature is called emissivity ε. All real materials have emissivity less than one, and it is among other things a function of wavelength, angle of radiation, temperature and surface roughness, but in practice it can often be treated as a constant. Especially when the emissivity is assumed to be independent of the wavelength, the shape of the object's emission spectrum is equivalent to the spectrum of a black body. This is known as the gray body assumption. The emissivity of real black body cavities is typically greater than 0,99. [16]

Total radiant emittance of a black body, in other words, the total power radiated per unit surface area of a black body, can be derived by integrating Planck law over all wavelengths and over the half-sphere solid angle. The result obtained is known as the Stefan-Boltzmann law

$$M_e = \sigma T^4 \,, \tag{2.7}$$

where σ is the Stefan–Boltzmann constant, defined as

$$\sigma = \frac{2\pi^5 k_B^4}{15c^2h^3} \approx 5{,}670\,373 \cdot 10^{-8}\ \mathrm{J{\cdot}s^{-1}{\cdot}m^{-2}{\cdot}K^{-4}} \,. \tag{2.8}$$

Real objects, however, do not emit all the power and therefore the emissivity of the material has to be taken into account. In the case of a grey body, Stefan-Boltzmann law takes the form

$$M_e = \varepsilon\sigma T^4 \,. \tag{2.9}$$

If the body is in an enclosure, such as a cavity or a room having a temperature T_{ext}, it will both radiate and absorb energy. The net radiant flux, or the net radiant power, of a source area of A_s becomes then [17]

$$\Delta\Phi_e = \varepsilon\sigma A_s(T^4 - T_{ext}^4) \,. \tag{2.10}$$

2.2.2 Incandescent sources

Incandescent light sources are most used in the near and mid infrared region. At longer wavelengths, a fundamental problem raises from the conflict between Wien's displacement law and Stefan-Boltzmann law described in equations 2.5 and 2.7, respectively. In order to spectral radiance peak at longer wavelengths, the temperature should be lower. This in turn strongly reduces radiant emittance. Nevertheless, at shorter wavelengths incandescent sources are irreplaceable.

Most incandescent light sources, such as the common light bulb, are based on a tungsten filament. The lamps are protected from air by glass envelope that is either evacuated or filled with inert gas. Lamps usually operate in the area of 1400 – 2400 K [11], but for special purposes much higher temperatures can be used – with inevitable cost of shortened lifespan, the absolute upper limit being the melting point of tungsten at

3695 K [13]. Spectral power of a common commercial infrared lamp is illustrated in figure 2.4.

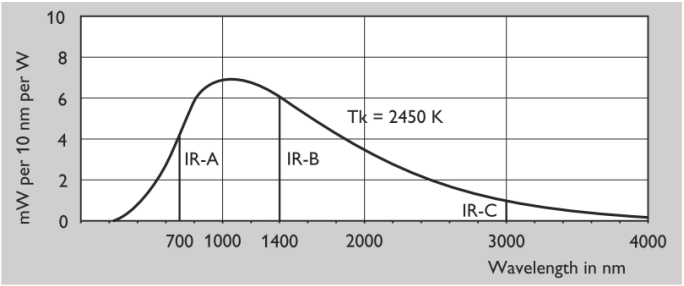

Figure 2.4 Spectral power distribution of Philips IR R125 series infrared lamps at the nominal filament temperature of 2450 K. [18]

The problem with standard tungsten filament lamps is evaporation on the filament. The higher the temperature is, the faster the process. The evaporated tungsten builds up to the inner wall of the bulb and affects the output of the lamp by absorbing some of the radiation. The filament itself also thins, causing the temperature locally to raise, filament to evaporate even more, and eventually to break. A halogen lamp, also known as the quartz-tungsten halogen lamp or the tungsten halogen lamp, offers a solution to this problem. It has a similar tungsten filament, but it is contained within a mixture of inert gas and some halogen gas. This halogen compound, for example iodine (I_2), methyl iodide (CH_3I) or hydrogen bromide (HBr), both combines with tungsten attached to the bulb and redeposit it back to the filament. This regeneration is known as the halogen cycle. Higher temperature causes the tungsten–halogen pair to decompose more rapidly, so the process automatically targets the thinnest points of the filament. Because higher filament temperatures can be used, halogen lamps are brighter and more efficient compared to normal tungsten lamps. Halogen lamps also have to be smaller in size, since the halogen cycle requires glass surface temperature to be at least 470 K, usually around 670 – 1300 K.

The glass envelope in a normal or tungsten filament lamp absorbs significantly radiation that has wavelength above 2,5 µm. The glass acts as a radiator itself, but naturally the surface temperature is far less than the filaments. The total spectrum of the lamp is

combination of these two spectra. The spectrum of a filament lamp can be improved with a special sapphire glass, which allows good spectral range up to 3 µm. [19]

Incandescent sources don't necessarily require any kind of enveloping glass. The simplest solution is merely using electrically heated resistance wire as an infrared source. This of course has a very limited temperature range, and therefore high radiances can only be attained briefly. A ceramic element on the other hand can operate well above 1000 K temperatures and have acceptable emissivity of 0,8 [20]. Spectral radiance of a commercial ceramic element is presented in figure 2.5. Some ceramic sources used originally for ignition purposes, reach temperatures around 1800 K [21]. Nernst glower is a similar, nowadays widely obsolete, device composed of a mixture of certain oxides. It does not conduct electricity at room temperature, but requires external start-up heating. One of its main replacements is a device alike, but made out of silicon carbine and commonly known as a globar. These devices make external heating unnecessary, function at a high temperature and have an emissivity as good as 0,88 [5].

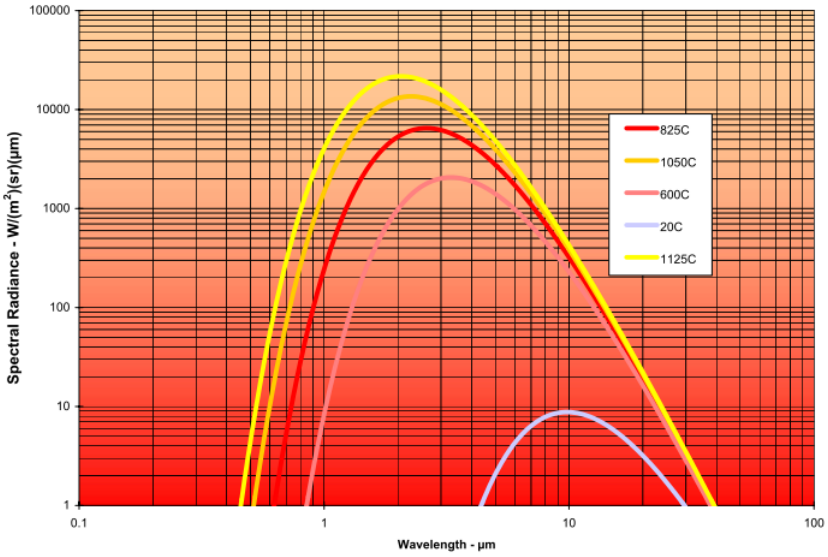

Figure 2.5 Spectral radiance of a ceramic element in different temperatures [20]. The peaks are noticeably narrower compared to a black body radiator.

Higher emissivity can be achieved with cavity blackbody radiators. They are based on a closed cavity with a small hole for output radiation. This structure captures almost all incident radiation, and when it is kept at a constant temperature it almost resembles an ideal black body; although for best performance the temperature and wavelength ranges might be rather limited. Nevertheless, black bodies with emissivity well above 0,999 have been reported [22], [23].

2.2.3 Other sources

Light emitting diodes for near infrared region have been long available. In fact the very first LEDs operated in the infrared region. Due advances in quantum technology and manufacturing, wavelengths up to mid infrared region are reachable. So called quantum cascade technology enables broadband emission in the infrared region. Originally these devices required low temperatures to operate, but LEDs have been reported to have emission in the spectral range of 5 – 8 µm at room temperature [24] and a flat band from 6 to 8 µm at low temperatures [25]. There is also a recent patent for multi-wavelength light source using various semiconductor elements that is specially designed for spectroscopy in the range of 650 – 2500 nm [26].

The very narrow spectrum of a common laser can be used for instance for calibration purposes in spectroscopy and there are devices available in the whole infrared region. Also broadband lasers are available, exploiting various quantum structures. Devices operating in the room temperature have been reported having continuous spectrum from 7,7 to 8,4 µm [27]. Supercontinuum generation on the other hand offers broadband radiation in optical fibers. Using this method, a broadband infrared source with emission up to 3,2 µm is demonstrated [28], while commercial applications with emission ranging from visible light to 2,5 µm are available [5].

Gas-discharge lamps, as the name suggests, send electric discharge through ionized noble gas or mixture of gases, usually mixed with other materials like mercury. Collisions between free electrons and atoms excite some of the electrons in atomic orbitals to a higher energy level, which then emit light at a material specific emission

lines. A special argon arc source has been designed for radiometric purposes. It is superior to incandescent infrared sources in the 1 – 10 µm wavelength region [29]. Cryogenic application can extend wavelengths up to 20 µm [30].

2.3 Considerations on infrared optics

The principles of optics are fundamentally the same in infrared region than in any other. Still, some special features have to be taken into account for instance in component and material selection. The infrared absorption of normal atmosphere is one major concern. This problem can be solved by using only suitable wavelengths, or performing the measurements in vacuum or in a purging gas, such as nitrogen. The latter solution of purging is also used in the measurement setup related to this thesis and is examined thoroughly in [4].

Absorption is also a problem in optical components. Lens materials commonly used in the visible region are rather opaque at longer wavelengths. There are many alternative materials in the near and mid infrared regions, many of which, though, are fragile, hygroscopic or toxic.

Many metals on the other hand have well known and flat reflectance over wide spectral range. Therefore reflective components are often a preferable option in the mid and far infrared regions. The reflectance spectrum of various metal coated mirrors is shown in figures 2.6 and 2.7.

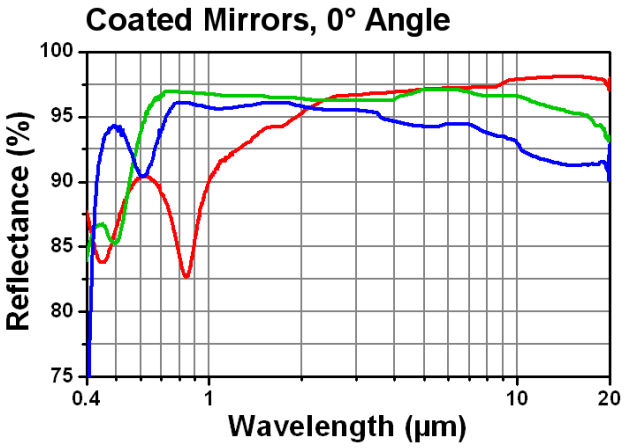

Figure 2.6 The reflectance spectra of aluminum (red), gold (green) and silver (blue) coated IR mirrors in 0° angle. [31]

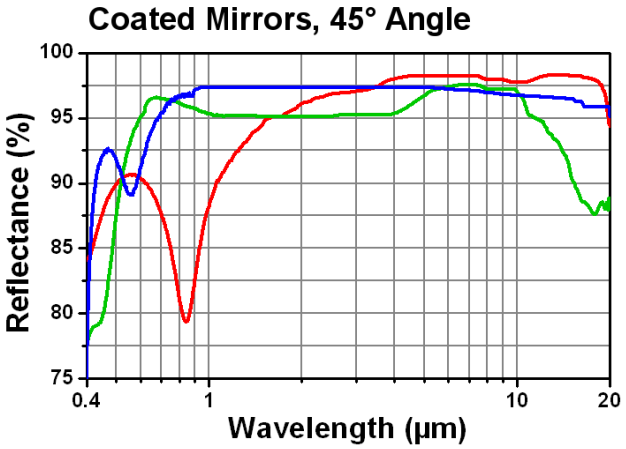

Figure 2.7 The reflectance spectra of aluminum (red), gold (green) and silver (blue) coated IR mirrors in 45° angle. [31]

With black coating materials the problem is completely opposite. These materials are used in components when reflection is unwanted, such as baffles and cavities. Materials that are very black in visible light usually are not in the infrared region. For most purposes commonly used optical blackout sheets, metal blacks, carbon based paints and polymers are good enough. For more demanding applications a surface treatment known as the super black can be used. This technique is based upon chemically etched nickel-phosphorus alloy. The reflectance is around one percent in the near infrared

region but rapidly increases thereafter [32]. The best blackbody material so far in a wide spectral range is a recently discovered nanotube structure, that has a remarkable reflectance of less than two percent in the 0,2 – 200 µm wavelength range. It is manufactured by growing a forest of vertically aligned single-walled carbon nanotubes on a silicon wafer [33].

A comprehensive overview of material selection regarding lenses, mirrors and black coatings in the infrared region can be found in [5].

2.4 Wavelength selection

This chapter outlines the most important principles and features of diffraction grating monochromator and filter based wavelength selection. More profound review on the matter can be found for instance in [10] or [11].

A monochromator uses a diffraction grating or a prism to separate a monochromatic beam from a broadband radiation. It acts as an optical band pass filter by focusing a small part of the spatially distributed light. The diffraction grating has multiples slits or grooves in a periodic configuration that creates a diffraction pattern of the incident light. This can be expressed mathematically with a so-called grating equation:

$$d(\sin\theta_i + \sin\theta_d) = m\lambda_m\,, \quad m \in \mathbb{Z}\,, \tag{2.11}$$

where d is grating constant or the distance between the grooves on the grating, θ_i is the angle of the incident light, θ_d is the diffraction angle, m is the diffraction order and λ_m is the corresponding wavelength. The reciprocal of the groove constant is known as the groove density. Figure 2.8 illustrates how multiple wavelengths with different diffraction order satisfy the equation. [10]

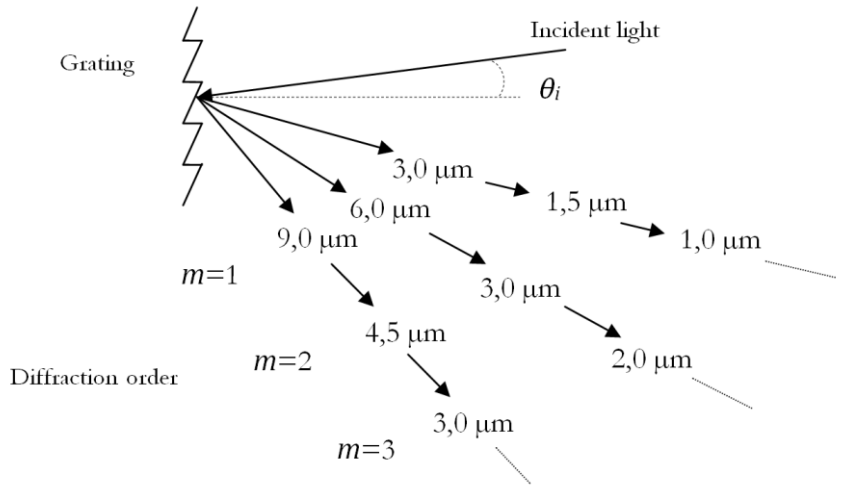

Figure 2.8 Illustration of the multiple solutions to grating equations with different diffraction order. [5]

The monochromator has a narrow but finite band pass. The spatial density of wavelengths in the diffracted distribution is called reciprocal linear dispersion ρ_y. It is measured in the plane of the exit slit transverse to the optical axis and is defined as

$$\rho_y = \frac{d\lambda}{dy}, \tag{2.12}$$

where y is the distance from the optical axis. The band pass B of the monochromator can now be approximated:

$$B = w\rho_y = \mathrm{w}\frac{d\lambda}{dy}, \tag{2.13}$$

where w is the width of the exit slit. Since the reciprocal linear dispersion is a function of diffraction angle, the approximation works best when the exit slit width is small. As a conclusion, smaller exit slit leads to narrower band pass, but of course the overall optical power decreases.

As a consequence of multiple wavelengths passing the monochromator, a set of filters is required to eliminate the unwanted wavelengths. Usually this is done using long wave

pass filters but in some cases a band pass filter might be beneficial. Infrared filters are typically made on a germanium substrate but in the near infrared region also silicon can be used. New type of plastic filters that have good thermal characteristics and tolerance for harsh chemical environment can be used close to visible light wavelengths [34]. The performance of a typical germanium based infrared filter is presented in figure 2.9.

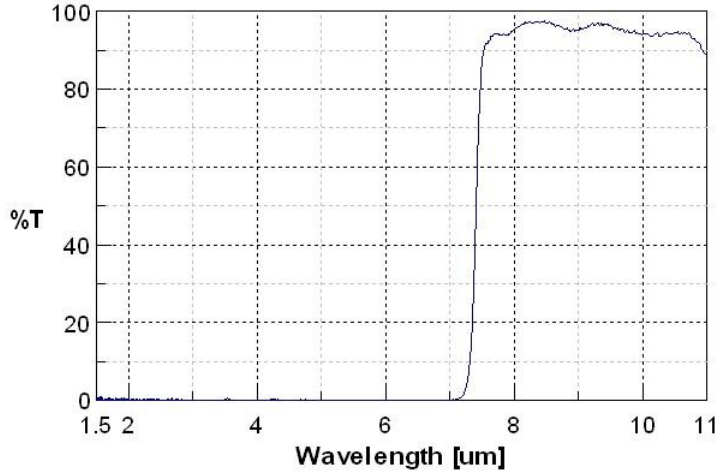

2.9 The performance of a typical infrared long wave pass filter on a germanium substrate. [35]

2.5 Detectors

Optical detectors measure optical power. Based on their operation principle they are generally divided into photomultiplier tubes, photon detectors and thermal detectors. The latter two are briefly discussed in the second and third subchapter, respectively, whereas photomultiplier tubes are beyond the scope of this work. All devices mentioned above are available for wide a range on radiation, but this thesis highlights the infrared region. Some general theory and important detector parameters are introduced in the first subchapter. More information on optical detectors at large can be found for instance in [10], [12] and [36], while [13], [37] and [38] focus on the infrared range detection.

2.5.1 Theory and definitions

A detector converts incident optical power P_{inc} to either output voltage V_{out} or output current I_{out}. Only detectors with voltage output will be discussed here, since all the equations apply when voltage terms are replaced by current terms. The responsivity of the detector *S*, also known as the photo sensitivity, is defined

$$S = \frac{V_{out}}{P_{inc}} . \tag{2.14}$$

If the irradiance E_e on the active area of the detector A_d is constant, one can simply assume

$$P_{inc} = E_e A_d . \tag{2.15}$$

In general, responsivity does not take the radiation spectrum into account. Therefore, it is defined in terms of suitability for application in question. For instance, the responsivities of infrared detectors are often measured with the spectrum of a 500 K black body. Spectral responsivity R_λ instead measures the wavelength dependence of detectors' response and is defined in terms of spectral power. The output of an ideal thermal detector is only dependent on the incident optical power and has therefore flat spectral response. The output of a photon detector on the other hand is dependent on the amount of incoming photons and has linearly increasing spectral response up to the cut-off wavelength λ_c. If the detector material has a band gap energy E_g, according to equation 2.1 we can determine the cut-off wavelength

$$\lambda_c = \frac{E_g}{hc} . \tag{2.16}$$

Noise equivalent power *NEP* is the quantity of incident power needed to equal the output and the intrinsic noise level of the detector, or in other words, it is the input power resulting to signal-to-noise ratio of one:

$$NEP = \frac{P_{inc}}{V_{out}/V_n} = \frac{V_n}{S} \tag{2.17}$$

where V_n is the noise voltage. Similar term noise equivalent irradiance NEI describes the performance of the whole system and is defined as the irradiance needed at the entrance aperture for the system output to have the signal-to-noise ratio of one.

The inverse of NEP is called detectivity D, which is proportional to the square root of detector active area and noise equivalent bandwidth of the measurement system B_n. Therefore, for detector comparison normalized detectivity is more convenient. The most used quantity is the specific detectivity D^*, that is defined as detectivity normalized to an effective area of 1 cm^2 and noise equivalent bandwidth of 1 Hz. It is expressed as

$$D^* = D\sqrt{A_d B_n} = \frac{\sqrt{A_d B_n}}{NEP} \tag{2.18}$$

and is typically measured in the unit of $cm \cdot s^{-½} \cdot W^{-1}$ [2]. A comparison of the specific detectivity of various commercially available infrared detectors and theoretical limits is presented in figure 2.10. The chopping frequencies used in the figure are 10 Hz and 1 kHz for thermal and photon detectors, respectively.

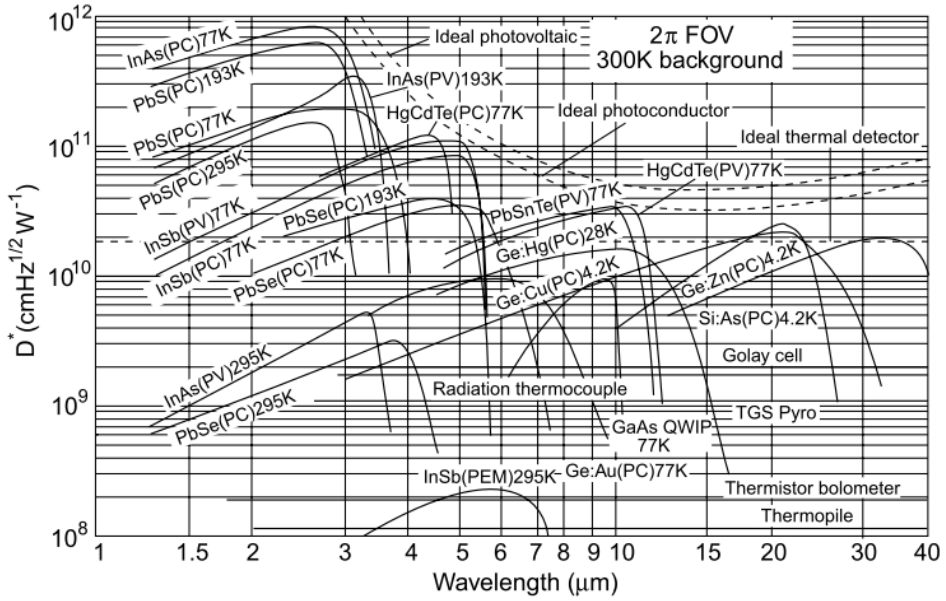

Figure 2.10 Comparison of the specific detectivity of various commercially available infrared detectors (solid lines) and theoretical limits (dashed lines). [38]

2.5.2 Photon detectors

Intrinsic, extrinsic and free carrier based semiconductor detectors together with quantum well and quantum dot structure based detectors are considered to be photon detectors. They all use electron excitation to detect incident radiation and have an absolute minimum energy level for detectable photon. The detection of small energy photons also requires cooling in order to reduce thermal oscillations in detection material. A simplified model of a general photon detector is presented in figure 2.11. Usually the optical area A_o and electrical area A_e are tried to be manufactured equal in size, but when the use of concentrator is possible, the ratio A_o / A_e can be increased.

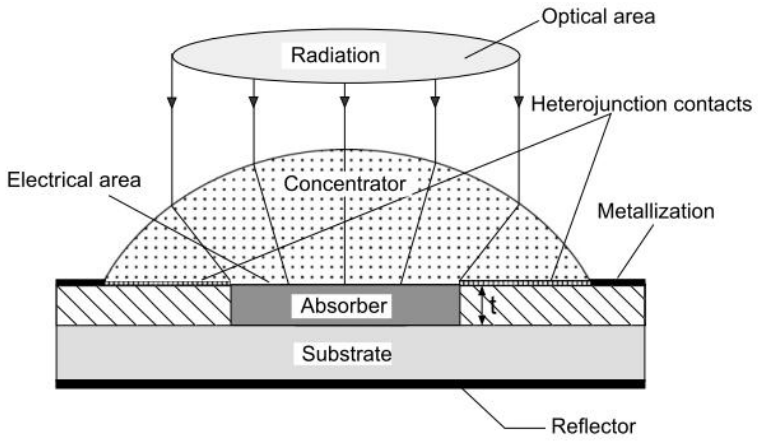

Figure 2.11 Model of a photon detector. [38]

Intrinsic detectors utilize the generation of electron-hole pairs across the semiconductor band gap in single semiconductor or a junction of semiconductors. Extrinsic detectors used doped semiconductor materials creating impurity states in the band gap, where charge carriers can transit. This allows photons with smaller energy to excite an electron. The disadvantage here is that thermal excitations are also easier and cooling to a low temperature is necessary. In free carrier detector the photon energy is absorbed by a free carrier in either conduction or valence band.

Advanced manufacturing techniques enable complicated quantum structures to be grown on semiconductors. These are based on bound states of an electron and hole, known as excitons. Confinement in one dimension is called a quantum well and confinement in all three dimensions is a quantum dot. Especially well structures have very important applications for example in space technology and thermal imaging. A quantum well infrared photodetector (QWIP) has been demonstrated in the range of 3 to 80 μm. A focal plane array (FPA) construction of QWIPs allows high performance imaging at long wavelengths [39]. Quantum dot infrared photodetectors (QDIP) have also been commercialized for infrared imaging devices and are feasible in high speed operations [40].

Photon detectors can also be divided into groups by operational mode, which are photovoltaic, photoconductive, photoemissive and photoelectromagnetic (PEM). Most

materials mentioned above can be used in different modes of operation. Photovoltaic detectors have a semiconductor junction, where a photon absorbed in the depletion region excites an electron from the valence band to the conduction band. This creates a potential difference at the junction and current can flow in a closed circuit. Photoconductive detectors on the other hand do not have a semiconductor junction and require external voltage across the detector. The electron excitation by absorbed photon then changes the measured resistance of the detector. Photoemissive detectors are based on the photoelectric effect, where electrons are emitted from matter as a consequence of photon absorption. Typical construction is a metal and a semiconductor junction that creates Schottky barrier. An avalanche photodiode (APD) is a photoemissive detector that provides high gain by generation of secondary charge carriers. PEM detectors exploit the photoelectromagnetic effect, where the photon absorbed by the semiconductor in a magnetic field generates electric current. [38]

2.5.3 Thermal detectors

Thermal detectors operate on the principle that incoming radiation increases their temperature. Temperature changes are then measured by a temperature-dependent mechanism, such as thermoelectric voltage, pressure or resistance change or pyroelectric voltage. Due to this energy conversion process, thermal detectors are generally slower and require higher power levels than photon detectors. In turn they can operate at room temperature, are relatively low cost and usually rugged, reliable and in principle, do not have spectral dependence in responsivity. [38]

Most common type of thermal detectors is the pyroelectric. Detector makes use of pyroelectric materials that become polarized when heated, much the same as piezoelectric material becomes polarized under pressure. This generates a tiny electric current that can be amplified and measured. The polarization charges will eventually drain, making the pyroelectric material neutralized. Therefore constant or very slowly modulated radiation cannot be measured.

Thermopile detectors exploit the thermoelectric phenomenon, where two different conductors generate a voltage proportional to a temperature gradient. Many thermocouple junctions can be furthermore connected in series to multiply the output level. The response time of a thermopile is typically around milliseconds, but it can be improved by reducing the active element volume. Semiconductor thermopiles have a higher sensitivity, but the traditional metal connectors are found to be more suitable for photometry.

Bolometers use temperature dependent resistance for detection. Semiconductors or biased active component are typically used to achieve high temperature coefficient of the resistance. Also some kind of heat absorbing mechanism is needed. The response time of a bolometer can be adjusted with the design of the heat sinking, but it is around milliseconds. Cryogenics cooling of the detector improves sensitivity and noise characteristics, but is not mandatory.

2.6 Signal amplification

Signal amplification itself is a vast science, so the subject has been narrowed down to two amplifiers most relevant to the thesis. The basic theory of lock-in amplifiers is discussed in section 2.6.1, and the various lock-in related electrical measurements that were conducted are presented in chapter 4. Section 2.6.2 deals with the theory related to the amplification of photoconductive detector's signal. Such a device was designed and built as part of this thesis, and is closely examined in chapter 6.

2.6.1 Lock-in amplifier

A lock-in amplifier is a device that uses a phase sensitive detection method, and enables the detection of very small signals in the presence of overwhelming noise. The method requires the signal source to be modulated at a known constant reference frequency. A simplified block diagram of a lock-in amplifier is presented in figure 2.12. For clarity various filtering and amplifications stages found in real devices have been omitted in

this theoretical model. The multiplier stage of the lock-in amplifier is commonly referred as a phase sensitive detector (PSD). [41]

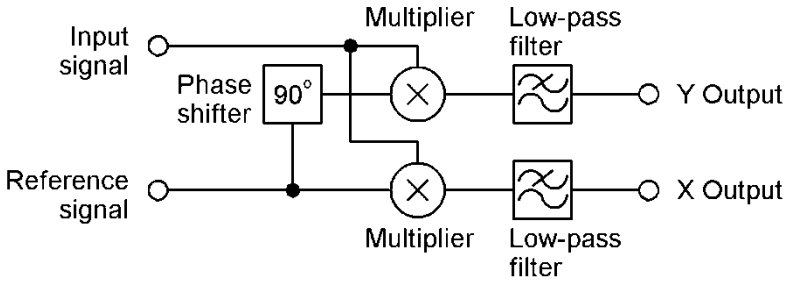

Figure 2.12 Simplified block diagram of a lock-in amplifier.

The reference signal u_r is a sine wave with an amplitude A_r and angular frequency ω_r. The phase shifter is used to generate another reference signal $\tilde{u}_r$ with 90° or π/2 radians phase difference

$$u_r = A_r \sin(\omega_r t)\ , \quad \tilde{u}_r = A_r \sin\left(\omega_r t - \frac{\pi}{2}\right). \tag{2.19}$$

The input signal u_{in} is a sum of a possible very large noise component u_n and the desired measurand signal u_m, that has an unknown amplitude A_m, and is being modulated with reference frequency ω_r. The measurement setup may cause a delay between reference and measured signal, which is seen as phase shift φ_m

$$u_{in} = u_m + u_n = A_m \sin(\omega_r t - \varphi_m) + u_n\ . \tag{2.20}$$

Using trigonometric identities one can obtain the result from input and reference signal multiplication

$$u_r u_{in} = \frac{A_r A_m}{2}[\cos\varphi_m + \cos(2\omega_r t + \varphi_m)] + u_n \sin\omega_r \tag{2.21}$$

$$\tilde{u}_r u_{in} = \frac{A_r A_m}{2}[\sin\varphi_m + \sin(2t\omega_r t + \varphi_m)] - u_n \cos\omega_r\ . \tag{2.22}$$

The multiplied signals are then being filtered with low-pass filter. When the cut-off frequency is much lower than the reference frequency, ideally only DC signal is left. The outputs X and Y can then be expressed as

$$X = \frac{A_r A_m}{2} \cos \varphi_m \tag{2.23}$$

$$Y = \frac{A_r A_m}{2} \sin \varphi_m \ . \tag{2.24}$$

So called magnitude *R*, which is directly proportional to the amplitude of the measured signal, and phase of the measurement signal can now be calculated from the output values:

$$R = \sqrt{X^2 + Y^2} = \frac{A_r A_m}{2} \tag{2.25}$$

$$\varphi_m = \tan^{-1}(Y/X) \ . \tag{2.26}$$

Usually these values are computed in the lock-in amplifier, but if very rapid sampling is needed, the calculation from *X* and *Y* values can be done later. For most devices *X*, *Y* and *R* are scaled so that they represent the RMS value of measured signal. Usually one can also measure the signal level at harmonic multiples of the reference frequency. [41]

The phase sensitive detection can be done either analogically or digitally. Modern digital lock-in amplifiers outperform analog counterparts in virtually all respects. The main problems in analog multiplication are related to insufficient harmonic rejection, output offsets, errors in the gain and rather limited dynamic reserve.

Instead of gain, the term sensitivity is used to characterize the amplifications of a lock-in amplifier. It is simply the full scale reading of the measured signal, somewhat similar to a range in a multimeter. When using digital PSDs, averaging allows measurements of signal levels even below one bit resolution. If *N* is the amount of measurement samples, uncorrelated noise is reduced by a factor of 1/*N*. Oversampling an AC signal is rather complicated, but since the filtered output of a PSD can be assumed constant, output

resolution simply increases by a factor of *N*. In essence, doubling the amount of measurement samples adds one bit to output resolution. [42]

Traditionally dynamic reserve is defined as the ratio of the largest tolerable noise to the full scale signal. However, in case of digital PSD this definition is not practical, because as mentioned above there is no unambiguous limit to resolution. Instead, dynamic reserve refers to the distribution of gain between the analog preamplifier and digital multiplication. For optimum performance, dynamic reserve should be as small possible, just enough to avoid noise voltage to overload any part of the device. [42]

2.6.2 Amplifier for photoconductive detectors

When an electric potential is applied across the absorbing region of a photoconductive detector and the energy of an incoming photon exceeds the energy gap between the valence and the conduction band, a current I_{det} proportional to the irradiance flows through the detector [43]. The detector also has a certain dark resistance R_D and corresponding dark current I_D. The output signal from a photoconductive detector is commonly extracted as voltage V_O by using a load resistor R_L and bias voltage V_B as shown in figure 2.13 [44].

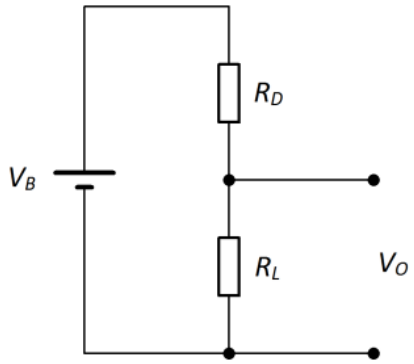

Figure 2.13 Model for extracting the output signal of a photoconductive detector using load resistor R_L and bias voltage V_B.

When the detector is not illuminated, the output voltage V_O is simply

$$V_O = \frac{R_L}{R_L+R_D} V_B \ . \tag{2.27}$$

A change in output voltage ΔV_O due changes in R_D when detector is exposed to light can be approximated with differentiation:

$$\Delta V_O = \frac{\partial V_O}{\partial R_D} \Delta R_D = -\frac{R_L V_B}{(R_D+R_L)^2} \Delta R_D \ . \tag{2.28}$$

The output voltage sensitivity has a maximum value $\Delta V_{O,max}$ when R_D and R_L are equal:

$$\Delta V_{O,max} = \Delta V_O|_{R_D=R_L} = -\frac{V_B}{4R_L} \Delta R_D \ . \tag{2.29}$$

In order to optimize the output signal level of the photoconductive detector, the load resistance should be well matched. By dividing equation 2.28 with equation 2.29, the efficiency of the detector due to resistor matching η can be calculated:

$$\eta = \frac{4\alpha}{(1+\alpha)^2} \ , \tag{2.30}$$

where α is the ratio R_L/R_D. The relation between the output efficiency and the ratio α is shown in figure 2.14. Because the dark resistance values of the detectors can vary enormously, the amplifier has to either be dedicated to one type of detectors or the load resistance should be selectable. Typical decade selection of resistors provides the minimum efficiency of about 73 %, while two resistors per decade increases the minimum efficiency to about 92 %.

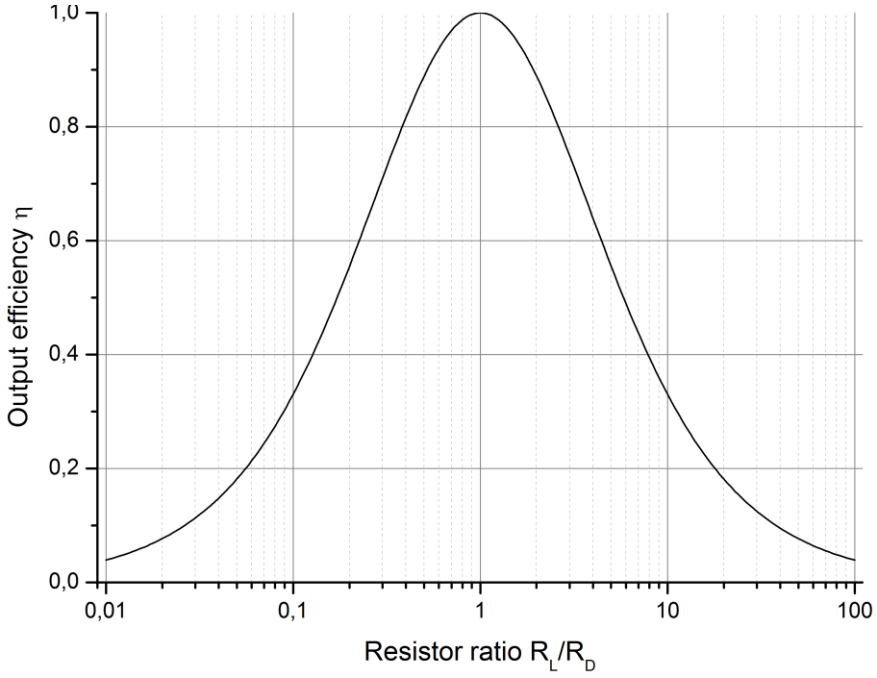

Figure 2.14 The relation between the output efficiency and the resistance ratio R_L/R_D.

As seen in equations 2.28, the output sensitivity of the detector is also directly proportional to the bias voltage. Therefore, it is usually beneficial to use as high bias voltage as the detector can withstand. However, there are some exceptions; lead selenide and lead antimony detectors have a specific threshold level for bias voltage, after which the noise levels suddenly rise. So, the bias voltage should not be any higher than necessary. In some cases the heating of detector element due higher bias voltage causes a problem as the D^* decreases, even the detector itself can endure [44]. In such cases the manufacturer usually recommends the optimum biasing voltage range.

With mercury cadmium telluride (MCT) detectors the bias current is more important factor than bias voltage or load resistance matching. Load resistance is usually in the range of kilo-ohms and the bias voltage is adjusted to achieve the wanted bias current. Figure 2.15 shows typical signal and noise behavior of MCT detectors as a function of bias current. [44]

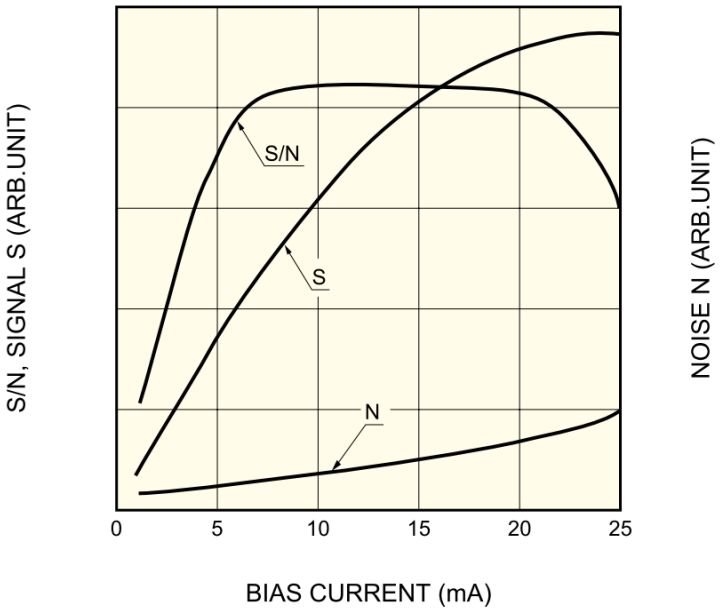

Figure 2.15 Typical signal and noise behavior of MCT detectors. [44]

3 Setup description and improvements

This chapter introduces the infrared spectrometer measurement setup. The main focus is in the improvements done as part of this thesis. For more profound description of the setup the reader is advised to look at the previous theses [3], [4] and [5]. The developed computer control of the devices and the automation of the measurement setup are described in the next chapter.

3.1 Setup overview

Figure 3.1 presents the overall layout of the measurement setup and an illustration of the electrical signal paths. Device controllers and computer connections are omitted from the figure for clarity. Table 3.1 explains the abbreviations used in the schematic diagram. The whole setup is built inside three airtight boxes made of polypropylene; this enables nitrogen purging when it is needed to avoid atmospheric absorptions. Cable glands are avoided by using airtight feed-through connectors; BNC connectors are used for measurement signals, DE9 connectors for device control and banana connectors for high current power supply.

Table 3.1 Abbreviations used in the layout diagram of the measurement setup in figure 3.1.

Abbreviation	Meaning
CM	Concave mirror
G	Diffraction grating
IRS	Infrared source
M	Flat mirror
OPM	Off-axis parabolic mirror
PS	Power supply
RD	Reference detector
SM	Spherical mirror
TD	Test detector
T/H	Thermohygrometer

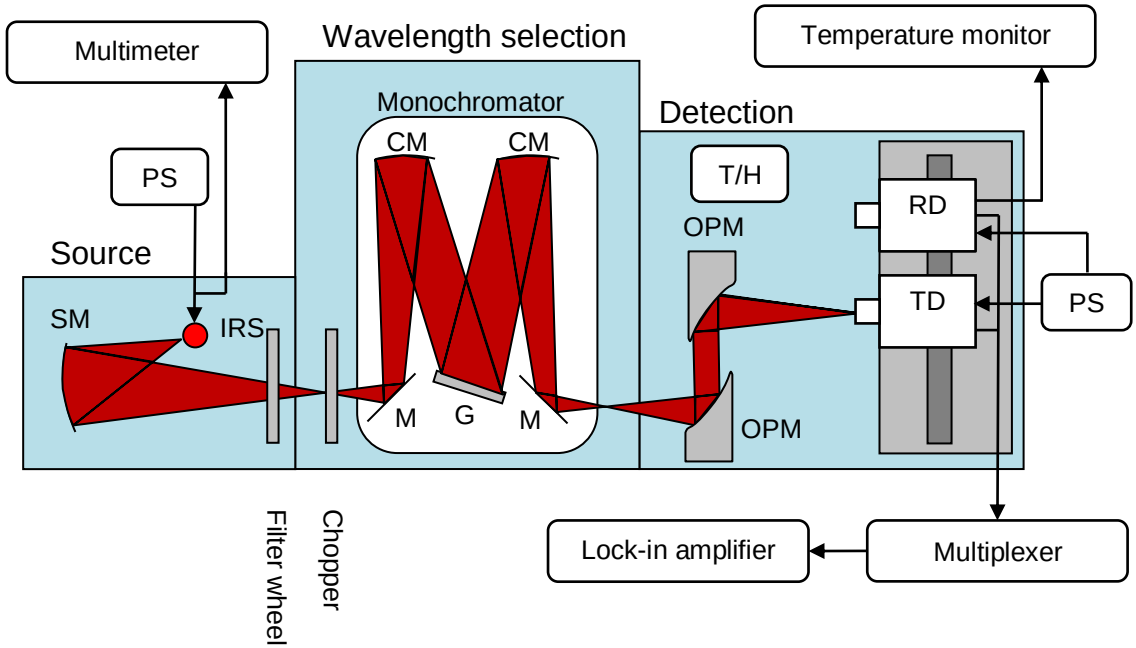

Figure 3.1 The layout of the measurement setup and an illustration of the electrical signal paths.

The spherical mirror is used to collect and focus the radiation from the infrared source to the monochromator through a filter wheel and an optical chopper. Light travels through a one inch wide zinc selenide window from a box to another. The optical chopper is placed in front of the entrance slit of the monochromator. The desired wavelength is then focused to the exit slit of monochromator. The beam travels through another optical window to the detection box. The two off-axis parabolic mirrors are used to collimate and focus the beam to the detector plane. Detectors are mounted on a linear detector stage, so that the reference detector and detector under measurement can be, in turn, placed and fine adjusted to the beam. This substitution method is thoroughly analyzed in [3].

As a part of the setup improvement all measurement and control devices were mounted to a standard 19 inch rack cabinet shown in figure 3.2. The tag numbers refer to devices listed in the table 3.2. All devices except the computer and its display are powered via rack power strip. This allows the setup to turned on and off with a single flick of a switch. The computer and its accessories are connected to a different phase in the power

grid, so that the disturbances caused by the switched-mode power supply could be avoided. Also most data and power cables run behind the devices while signal cables are in front, so as to minimize noise. In order to simplify data wirings, all device communications were implemented with a USB hub and various interface adapters that were placed behind the display. These connections are further explained together with setup automation in chapter four.

Table 3.2 List of measurement and control devices mounted to the rack shown in figure 3.2.

Tag	Device	Model
1	Cooling fan unit	Self-made
2	Linear translator controller	Self-made
3	Rack main power switch	Adam Hall 87471
4	Monochromator controller	МДР-23
5	Power supply	elc AL 924A
6	High voltage supply	Stanford PS325
7	Multimeter	Agilent 34410A
8	Lock-in amplifier	Stanford SR830
9	Filter wheel controller	Optec IFW
10	Optical chopper controller	Terahertz Technologies C-995
11	Power supply	Instoma TL201
12	Precision attenuator	Self-made
13	Signal generator	Agilent 33521A
14	Linear translator controller	isel IT116 flash
15	Computer and accessories	

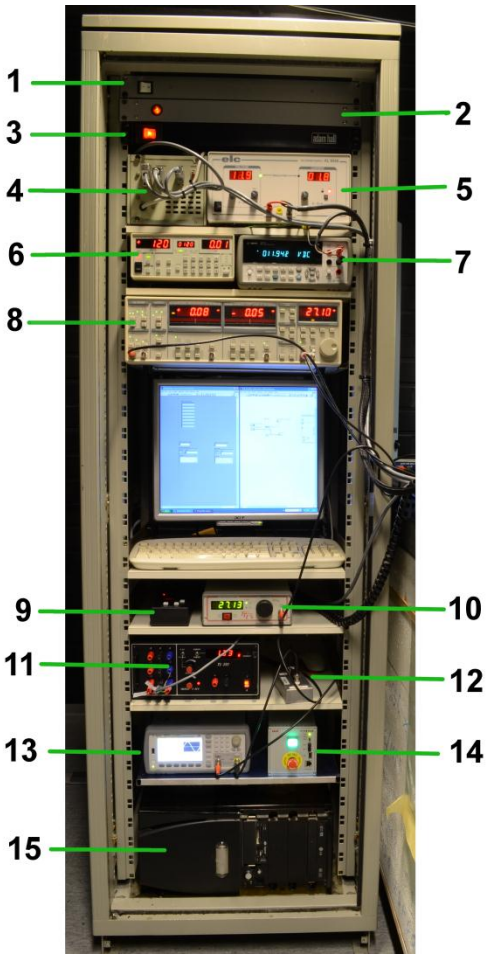

Figure 3.2 Measurement and control devices mounted to a standard 19 inch rack cabinet.

The monochromator controller (number 4 in figure 3.2) and the high current power supply (5) tend to heat a lot even when they are not active. Therefore, they were placed under a cooling fan unit (1), which circulates air through the whole rack cabinet. The cooling unit consists of four air fans and a variable transformer, so that the rate of the airflow can be adjusted.

The signal generator (13) and the precision attenuator (12) are actually not part of the spectral responsivity measurement setup. Originally they were used to characterize the electrical properties of the setup. However, they were left as a part of the setup, as they provide a simple and fast auto-calibration method for the phase sensitive measurement.

3.2 Radiation sources and input optics

The primary source of infrared radiation in the setup is a ceramic glower model Mini−Igniter™ 301 manufactured by the Saint-Gobain Ceramics. Individual glowers have significant differences in the material properties; at the nominal 12 V operating voltage the steady-state current can vary from 1 to 2,4 A. This in turn leads to the temperature range of 1150 – 1455 °C. More important factor is the power dissipation of the glower, which can be adjusted by fine tuning the operation voltage. The maximum rated temperature of the device is 1580 °C [21]. Assuming that the glower is roughly a gray body, the Wien's displacement law in equation 2.5 predicts the spectral radiance to peak around 2 µm region when the glower is used in the nominal temperature range.

The previously used glower was damaged and had to be replaced with a new one. The dimensions of the new version glower were unfortunately changed, even though the model number is the same. The actual glowing tip has the same dimensions, but the holder part is significantly larger. Due to this a new holder was machined on the basis of the old one. Also a fitting piece was made that enables the smaller version of the glower to be used as well. The new holder and the glower in operation are shown in figure 3.3.

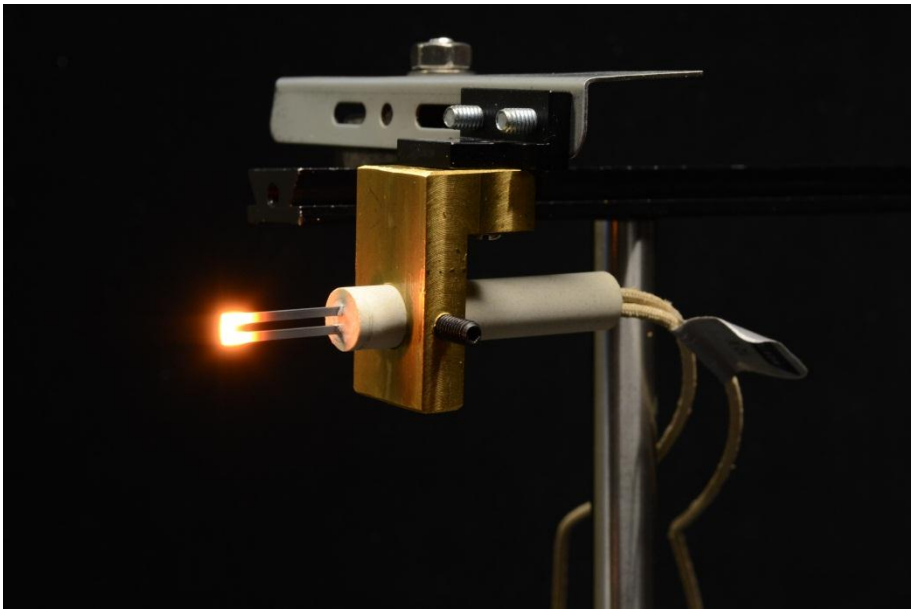

Figure 3.3 The new holder and the ceramic glower in operation.

The ceramic glower can be used as an infrared radiation source up to 16 µm. For near infrared operation a halogen lamp can be used. The model commonly used in the setup is a 50 W Osram Halostar that peaks its optical power around 1,2 µm [3]. It provides a good source of infrared radiation up to 2,5 µm, after which the glass envelope starts to absorb the radiation [4].

Both radiation sources use the same power supply. Mastech HY3005D regulated power supply was previously used in the setup. However, the device in question was measured to be surprisingly noisy, having a root-mean-square ripple well above the nominal 500 µV [45]. The test measurement was done driving 12 V into an 8 Ω load. It was then replaced with an *elc* AL 924A power supply, which is capable of providing voltage up to 30 V and current up to 10 A. Higher current rating enables higher power light sources to be used in the future. According to specifications, the absolute maximum ripple of the device is 1,8 mV RMS and 5 mV peak-to-peak even at maximum current [46]. A similar ripple measurement was conducted and the new device performed very well; the RMS noise was less than 100 µV.

The old cabling from the power supply to the infrared source was replaced with a thicker 4 mm^2 cable in order to decrease the voltage drop. In addition to that, separate voltage sensing cables were installed, so that the actual operating voltage of the source can be monitored with a multimeter to compensate the voltage drop in the cables.

A concave spherical mirror made of aluminum and a protective layer of magnesium fluoride is used to collect the radiation from the glower. The diameter of the mirror is 93 mm and the focal length 125 mm. The distance from the source to mirror is 165 mm and it focuses the light to the entrance slit of the monochromator at a 455 mm distance. This magnifies the source by a factor of about 2,8 making the image of the 1,3 mm wide tip of the ceramic glower barely fulfill the 3,6 mm wide entrance slit of monochromator.

3.3 Wavelength selection and chopping

An eight position IFW filter wheel from Optec Inc. with a set of long wave pass filters is used in front of the monochromator. This prevents the pass of unwanted diffraction orders through the monochromator. Table 3.3 presents the current order of the filters and their specification.

Table 3.3 Filter wheel arrangement and working regions. [5]

No.	Cut-on wavelength (5%)	Working range	Substrate	Part-number
1	Open aperture	-	-	-
2	Closed aperture	-	-	-
3	1,05 ± 0,04 µm	1,2 – 2,0 µm	Si	LOT-Oriel 50829-FK
4	1,65 ± 0,07 µm	2,0 – 2,7 µm	Ge	LOT-Oriel 50830-FK
5	2,40 ± 0,09 µm	2,7 – 4,0 µm	Ge	LOT-Oriel 50831-FK
6	3,60 ± 0,14 µm	4,0 – 6,0 µm	Ge	LOT-Oriel 50832-FK
7	5,60 ± 0,10 µm	6,0 – 10,5 µm	Ge	BARR A36
8	10,30 ± 0,10 µm	10,5 – 16,0 µm	Ge	BARR X0041

Terahertz Technologies C-955 optical chopper is placed in front of the monochromator. It should be as close to the entrance slit as possible, since this minimizes the loss caused by the finite aperture of the chopper. This also guarantees sharp rectangular shape of modulation even with low chopping frequencies.

The chopper has two apertures, inner and outer, with frequency ranges of 4 – 500 Hz and 40 – 5000 Hz, respectively. Both provide the 0,01 % accuracy and 1 mHz resolution. Normally only the inner aperture is used, since it provides smaller phase jitter, shorter rise and fall time of chopped optical signal and larger beam diameter.

The most important part of wavelength selection is the Czerny-Turner type monochromator МДР-23. It was originally built to cover working range of 200 – 2000 nm [47], but the range has been extended by purchasing new gratings with smaller groove frequency. All available gratings and their properties are listed in the table 3.4.

Table 3.4 Available gratings and their properties. Original accessories of the monochromator are underlined. [5]

Grating	Groove frequency [lines/mm]	Working range [µm]	Type	Scaling factor
G1200 I	1200	0,2 – 0,5	Ruled	1
G1200 II	1200	0,35 – 1,0	Ruled	1
G600	600	0,7 – 2,0	Ruled	2
G300	300	1,5 – 4,0	Holographic	4
G150	150	3,0 – 8,0	Ruled	8
G75	75	6,0 – 16,0	Ruled	16

The monochromator can be driven manually or with an external controller. The external controlling is simply done by giving clock pulses to the driver of the stepper motor rotating the grating. With the scaling factor of one the theoretical resolution is 3 pm per clock pulse. For computer controlling via serial port a custom made controller is used [48]. It was working inconsistently until a large filtering capacitor was added to the supply voltage taken from the monochromator. The device uses a first degree polynomial function to compute the needed amount of pulses to drive the monochromator to a wanted wavelength, although separate clock pulses can also be driven. A more sophisticated nonlinearity correction of the monochromator is done in the computer program either by a higher degree polynomial function or spline function. For instance a narrow bandwidth laser can be used as a calibration source. Without filters all diffraction orders are seen in the output and the whole scale can be calibrated. The nonlinearity correction functions are further discussed in section 4.1.2.

3.4 Output optics and detection

3.4.1 Output optics

The output beam of the monochromator travels through a zinc selenide window to the third polypropylene box. The window has an antireflection coating, which improves the transmittance to approximately 80 percent in the wavelength range of 1 to 15 µm. The

beam is diverging at this point, but it is then collimated with a bare gold coated off-axis parabolic mirror placed at its focal length 152 mm from the monochromator exit slit. Another similar mirror is used to focus the beam to the detector plane. A linear translator is used to change detectors in the detection plane.

3.4.2 Pyroelectric reference detector

A hybrid pyroelectric detector SPH-49 from Spectrum Detector, shown in figure 3.4, is used as a transfer standard for infrared responsivity measurements. The device consists of a large lithium tantalate $LiTaO_3$ pyroelectric element and a 100 GΩ transimpedance amplifier. The detector was previously characterized up to 13 µm and was found to be very linear as expected. Detector's spectral responsivity in the wavelength range of 2,8 to 6 µm is shown in figure 3.5. In order to link the spectral responsivity of the pyroelectric detector, the method of substitution was used to compare the pyroelectric detector with the primary reference at wavelengths of 3 and 5 µm [5]. The primary reference is an electrically calibrated pyroelectric radiometer (ECPR) that is traceable to a cryogenic radiometer via comparison with silicon trap detectors [49].

Figure 3.4 Hybrid pyroelectric detector used as a transfer standard for infrared responsivity measurements. In the left side picture a hemispherical reflector is used for reflectance correction.

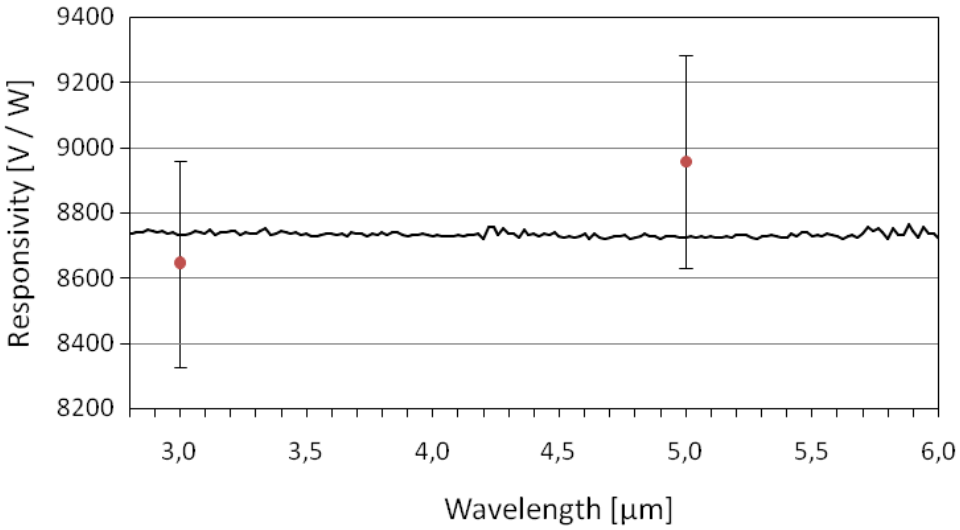

Figure 3.5 Spectral responsivity of the transfer standard between 2,8 and 6 µm measured at 15 Hz chopping frequency. The data points shown as red dots were obtained by comparing the responses of the transfer standard and the primary reference. [5]

The frequency response of the transfer standard, on the other hand, is known to be very poor [50]. To confirm this behavior and to acquire more accurate correction coefficients, the relative responsivity was measured at low chopping frequencies from 4 to 15 Hz, shown in figure 3.6. Values are compared to the responsivity at 15 Hz chopping frequencies, which is also used in the comparison measurements with the primary standard. More detailed documentation about the transfer standard is available in [5].

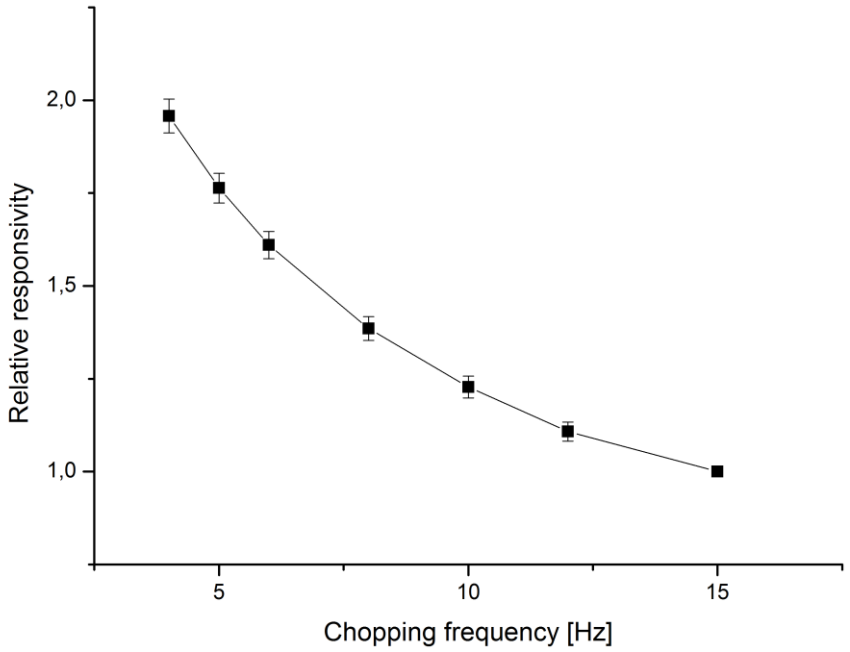

Figure 3.6 Frequency response of the transfer standard at low frequencies. Relative values are compared to the responsivity at 15 Hz chopping frequency.

Strong noise signal level at line frequency and its multiples has been reported previously to cause problems in measurements around same frequency range. This was confirmed by measuring the output signal of the detector with an oscilloscope when the input aperture was closed. Figure 3.7 shows the measured disturbance signal having a peak-to-peak voltage of over 500 mV.

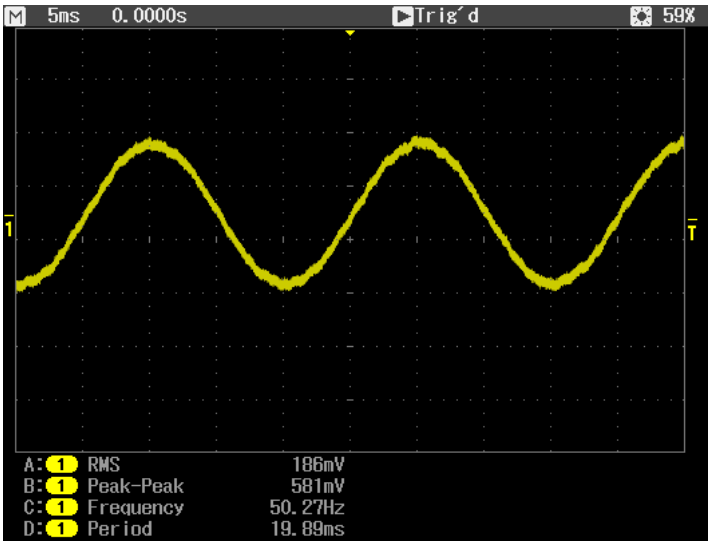

Figure 3.7 Output signal of the pyroelectric detector with blocked input aperture.

The preamplifier of the detector was supplied by a typical bench top power supply which seemed to cause most of the noise signal. Multiple power supplies were tested, but the proximity of the devices to the detector seemed to cause similar effect in any case. This is most likely due to the fact that the casing of the detector is connected straight to amplifier's ground potential. The problem was eventually solved by placing the power supply two meters away from the detector and placing an external RC filter network to supply lines close to the detector. The schematic of the filter is shown in figure 3.8 and the resulting output with the improved arrangement in figure 3.9. The level of the line frequency disturbance attenuated over 24 dB.

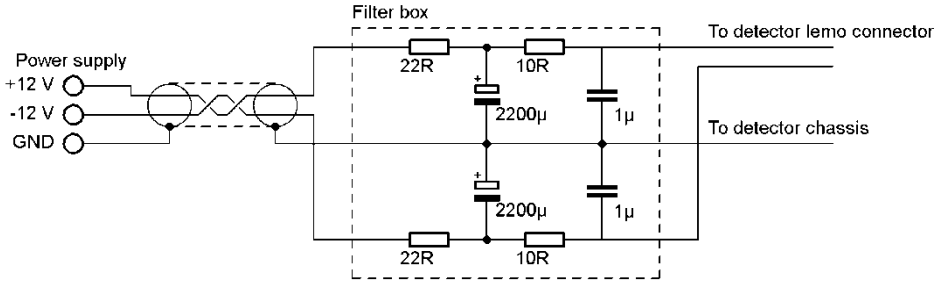

Figure 3.8 RC filter for the pyroelectric detector.

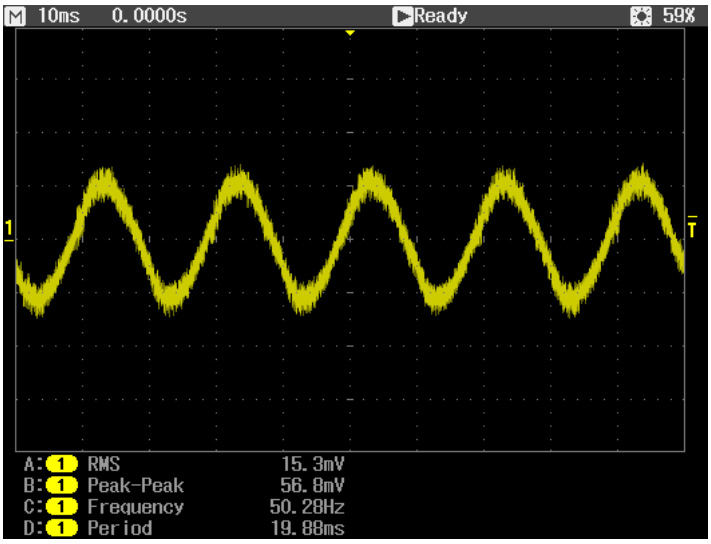

Figure 3.9 Output signal of the pyroelectric detector with blocked input aperture after installing the RC filter. The attenuated disturbance signal has a peak-to-peak voltage of about 60 mV.

Also has a high frequency noise component around 900 kHz was observed both with and without the supply voltage filtering. The signal, shown in figure 3.10, has a peak-to-peak voltage of around 3 mV. Fortunately this high frequency causes negligible error in the low frequency lock-in measurements.

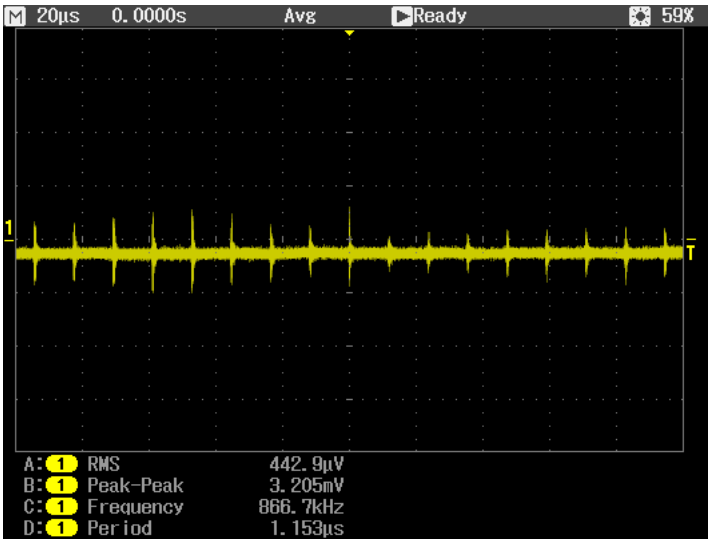

Figure 3.10 900 kHz disturbance signal measured at the pyroelectric detector output.

3.4.3 Other detectors

Various other detectors have been used in the setup, of which the most important ones are introduced in this section. The previous reference detector used in the setup was a pyroelectric radiometer RK-5700 from Laser Precision with an internal chopper. This device can still be used for instance in comparison measurements.

An indium arsenide photodiode model J12TE1-66D-R02M manufactured by the Judson Technologies was previously mounted to the integrating sphere, but is now used separately. The device has an internal preamplifier and thermoelectric cooling element. The colder the photodiode is kept, the higher the responsivity, but also the wavelength of the peak responsivity shortens. Typically measurement temperature is around -20 ˚C, corresponding to 7,7 kΩ resistance in the thermoelectric cooling element. This results in a peak wavelength of 3,3 µm. At longer wavelength the responsivity rapidly decreases.

Two photoconductive photodiodes, model P2038-03 lead selenide detector by Hamamatsu Photonics and model J13TE1-3CN-S01M lead sulfide detector by Judson Technologies, are also being used. These devices are compared in table 3.5.

Table 3.5 Comparison of the two photoconductive detectors used in the setup. [51], [52]

Manufacturer	Hamamatsu	Judson Tech.
Model	P2038-03	J13TE1-3CN-S01M
Material	lead selenide	lead sulfide
Temperature range [˚C]	-30 to +50	-30 to +50
Nomimal temperature [˚C]	-10	-10
Wavelenght range [µm]	1,5 to 5,1	1,0 to 3,5
Peak wavelength [µm]	4,1	2,5
Peak D* [cm·s$^{-½}$·W^{-1}]	$3 \cdot 10^{9}$	$1{,}5 \cdot 10^{11}$
Typical D* [cm·s$^{-½}$·W^{-1}]	$3 \cdot 10^{8}$	$1{,}5 \cdot 10^{9}$
Active area [mm^2]	3 x 3	10 x 10
Dark resistance [MΩ]	1,7 – 7,0	0,5 – 8,0
Nominal bias voltage [V]	50	240
Maximum bias voltage [V]	100	500

3.5 Other equipment

Whenever possible, built-in preamplifiers of the photovoltaic detectors are used. In other cases common current to voltage converter, such as Vinculum SP042 or Stanford SR570 are used. For photoconductive detectors on the other hand a versatile preamplifier was built, that is discussed in chapter 6. This device has an internal biasing possibility of up to 64 volts. For higher voltages Stanford Research PS325 supply is used as an external bias, which can provide DC voltage up to 2,5 kV and current up to 10 mA [53]. The output signals of various detectors and preamplifiers are routed to the lock-in amplifier via Signal Recovery 3830 multiplexer. It has six floating channels that can be used as either inputs or outputs and are coupled to one of two common buses [54].

The temperature and humidity of the detection box can be monitored during the measurement with a Vaisala HMI41 thermohygrometer. The temperature is measured with 0,2 °C accuracy and relative humidity with 2 % accuracy [55]. More important factor here is the stability of both values in comparison measurements. Some detectors have an internal temperature control, but in other cases the temperature of detector is controller with a Thorlabs TED200 temperature controller.

A step motor driven linear translator *isel* LES 5 is used in the detector plane. It was previously driven with a self-made controller based on the *escap* EDM-453 stepper motor drive circuit that allowed microstep operation up to 64 microsteps per full step, resulting in 25600 microsteps per revolution [56]. At this resolution, the movement was understandably agonizingly slow and because the stepping mode could not be changed, it was typically used without microstepping. The former controller had broken down, so a new controller was purchased. This new *isel* IT 116 Flash controller provides the same maximum resolution of 25600 microsteps per turn [57] and the resolution can easily be changed.

4 Setup automation

The first version of the measurement setup was controlled manually, but when nitrogen purging was introduced, the setup was automated for most parts. The original automation software was written in Java, but also used routines written in C and C++, external C++ libraries with Java Native Interface (JNI), dynamic link libraries (DLL), Windows ActiveX components and various native support packages. All in all, the software was rather complicated, platform-dependent, sometimes unreliable and laborious to modify and update.

When the development of the setup began, it became clear that various parts of the original code had to be rewritten, and also the old computer had to be replaced. As a part of the setup modernization the automation programs were decided to be rewritten with visual programming language LabVIEW from National Instruments (NI). It is a widely used system design platform and development environment very appropriate for device control and automation. It is also *de facto* standard in the laboratory measurements, since it provides a large selection of ready-made device drivers and data processing libraries. [58]

Unlike a set of compiled Java programs, LabVIEW allows very adaptive programming, so that built tools can be used with ease for any type of measurement. LabVIEW functions are coded as separate virtual instrument files or VIs that act as building blocks for new programs. A VI used inside another is commonly referred as a subVI. All code was written with LabVIEW 9.0f3, being the latest available version of the software available at the time.

4.1 LabVIEW device drivers

With the exception of preamplifiers, two power supplies and the cooling unit, all devices in the measurement setup are computer controllable. These devices along with their connection interfaces and used LabVIEW drivers are presented in table 4.1. For four devices LabVIEW drivers were not available and they were self-written. The

multimeter Hewlett-Packard 3458A is not part of the measurement setup *per se*, but it was used in various thesis related measurements and still provides a good tool for calibration measurements.

All devices lacking a LabVIEW driver were coincidentally connectable via RS-232 serial port. This allowed many of the same type VIs to be used in all the drivers with some modifications. The section 4.1.1 concerns general aspects of RS-232 interfacing and the other sections focus on the actual device drivers that were written.

Table 4.1 Device connections and used LabVIEW drivers. Drivers that were modified are underlined.

Device	Model	Interface	LabVIEW driver
Filter wheel	Optec IFW	RS-232	Self-made
Optical Chopper	Terahertz Technologies C-995	RS-232	Self-made
Monochromator	МДР-23	RS-232	Self-made
High voltage supply	Stanford PS325	GPIB	NI certified driver
Multiplexer	Signal Recovery 3830	USB	Signal Recovery
Lock-in amplifier	Stanford SR830	GPIB	NI certified driver
Multimeter	Agilent 34410A	GPIB	NI certified driver
Thermohygrometer	Vaisala HMI41	RS-232	Self-made
Linear translator	isel IT116 Flash	RS-232	Techno Linear Motion Systems
Signal generator	Agilent 33521A	USB	NI certified driver
Multimeter	Hewlett-Packard 3458A	GPIB	NI certified driver

4.1.1 RS-232 interface drivers

LabVIEW's built in communication tool called the Virtual Instrument Software Architecture (VISA) was used for serial connection. This takes care of the port settings, data flow and error handling. Most of device functions only require sending a command and then parsing the replied information. Therefore, all drivers share similar connection initialization and closing VIs, as well as message send and read VIs. In addition to VIs listed in this chapter many utility VIs were written to perform simple tasks. These are considered self-evident and are mainly excluded from the thesis.

The initialization VI is used to assign the serial connection related parameters. These are the speed of the connection (bits/s), buffer flow control and the number of data, parity check and stop bits. This is done using *VISA Configure Serial Port* VI. Also the possible usage of termination character is specified. Some devices require some start-up data or a command to enter remote mode. These are also sent by the initialization VI when necessary. In order to ensure stable operation, an appropriate delay is set before exiting the initialization VI.

The send and read VI sends a message to the device and waits for a possible reply. The reading of the reply may also be ignored when it is unnecessary. Before sending anything to the device the serial read buffer is emptied, since it tends to fill from unread replies. A specific timeout is also defined, which cancels the execution of the VI in case the connection is lost.

The connection closing VI sets the device to initial state and sends a command to exit remote mode when needed. Finally VISA Close subVI is used to terminate the connection and check whether any errors occurred.

4.1.2 Monochromator

Short descriptions of VIs related to controlling the monochromator are presented in table 4.2. *Get position* VI gives position of the monochromator and *Move to position* moves the monochromator to a given position. Also a given distance or a given number of stepper motor pulses can be moved with VIs *Move distance* and *Move pulses*, respectively. The *Stop* VI forces the movement to stop, and is the only command that can be given while other command is being executed. The monochromator controller uses linear correction, the parameters of which can be read with *Get gain* and *Get offset* and written with *Set gain* and *Set offset*. *Calibrate controller* is a standalone VI to read and write both parameters simultaneously.

The VIs listed above only utilize the linear correction done by the monochromator controller. Additional three VIs are available if more precise nonlinearity correction is

needed. Both require calibration data for the grating in question, which is read from user specified text file. Each line of the file must contain data in the form

<expected wavelength> *<measured wavelength>*

where both values are in nanometers and comma is used as a decimal mark.

Table 4.2 Descriptions of VIs related to controlling the monochromator.

VI name	**Description**
Initialize	Initialize connection
Send and read	Send commands and read replies manually
Close	Close connection
Get position	Read current position
Move distance	Move a given distance
Move pulses	Move the stepper motor a given number of individual pulses
Move to position	Move to a given position
Stop	Force all movement to stop
Get gain	Read the linear correction gain of the controller
Get offset	Read the linear correction offset of the controller
Set gain	Write the linear correction gain of the controller
Set offset	Write the linear correction offset of the controller
Calibrate controller	Read all linear correction data and if desired, write new values

Polynomial correction VI uses least squares method to fit polynomial correction function of given degree to calibration data, or manually given coefficients can be used with *Manual correction*. *Spline correction* VI on the other hand creates a spline function from given calibration data and uses it to interpolate corrected wavelengths.

4.1.3 Filter wheel

VIs used for filter wheel control are listed in Table 4.3. The VIs used for wheel movement are quite self-explanatory. *Select filter position* drives the wheel to a given position using shortest rotating route. *Select home* moves the wheel always clockwise and stops when it detects the first wheel position. This may take up to 20 seconds and is

necessary only if the device is moved both manually and in the remote mode. Other option is to use the *Get filter position* function to ensure current wheel position.

Table 4.3 Description of VIs related to controlling the filter wheel.

VI name	Description
Initialize	Initialize connection
Send and read	Send commands and read replies manually
Close	Close connection
Select home	Driver filter wheel to home position
Get filter position	Read current position of the filter wheel
Select filter position	Driver filter wheel to a given position
Identify wheel	Identify current filter wheel
Identify filter	Identify a given filter
Read wheel data	Read the whole data of the current filter wheel
Write wheel data	Write the whole data of the current filter wheel
Calibrate	Calibrate filter wheel movement

Many wheels can be used with one controller and therefore all wheels are given a letter identifier. Current wheel can be read with *Identify wheel* VI, which is useful if multiple wheels are being used. Also each filter is given a name, which can be read with *Identify filter* VI. All filter wheel data can be read at once with *Read wheel data* VI.

The wheel data is stored in the controller in a non-volatile EEPROM memory. The data has to be stored one byte at a time and storing one character takes about 25 ms. For this purpose a standalone *Write wheel data* VI was coded. It modifies the given text data to a suitable format and takes care of the storing process. For practical reasons, the wavelength ranges of the filters were saved as their names.

The filter wheel has an offset correction for both counterclockwise and clockwise movement. Basically this is a small angle correction to make sure that the filter always stays in the center of the device aperture. This is done using the *Calibrate* VI. To simplify the usage, correction values to factory presets are given instead of absolute values. The device used in the setup was verified working properly with correction value +2 clockwise and zero correction counterclockwise.

4.1.4 Other devices

The optical chopper is rather easy to control. In an addition to common initialization, manual command sending and closing VI, typical user only needs two additional VIs. The current status of the chopper is read with a VI *Get status*, which returns the selected frequency range, possible usage of external frequency source and current frequency. The first two parameters are only selectable via device front panel, but frequency can be set with the VI *Set frequency*. If the given frequency is not within the device's limit, the highest or lowest possible frequency is set.

The remote interface of the thermohygrometer is somewhat complicated, but using the device with LabVIEW was made really simple. When the connection is initialized, the device is automatically set to suitable measurement mode and kept there until connection is closed. All data handling is done using the *Get data* VI. The device sends all the data in one long string of which all the values are parsed. Most used are temperature and relative humidity, but also available are absolute humidity, dew point temperature, wet-bulb temperature, mixing ration and device battery voltage.

The high voltage supply uses NI certified drivers that are suitable for controlling all Stanford PS300 series voltage supplies. All except one VI of the driver worked seamlessly; the function for setting the voltage was evidently meant for different version of the device. The problem was remedied by partially rewriting the VI. So, instead of using the original *VI Set voltage*, one should use the modified version *Set voltage fix*.

4.2 Programs for electrical measurements

Various programs were written for electrical testing methods. The programs were also used to characterize the lock-in amplifier and these measurements are further discussed in chapter 5. Linearity measurements use Agilent 33521A signal generator and an attenuator to sweep voltage levels in decades to measure lock-in amplifiers linearity. Frequency response is measured by changing the frequency with the signal generator

within a given frequency range. All values are then saved to a comma-separated values (CSV) file, the name and folder of which are either given in advance or prompted at the end of the measurement.

Lock-in linearity VI measures the output of the lock-in amplifier using manually selected parameters, such as the time constant and settling time, at the given signal generator voltages and frequencies. The possible usage of attenuator is also specified. By default, the sensitivity range is optimized by the measurement VI, but it can also be selected manually or by using the auto-gain function of the lock-in amplifier.

Frequency response VI can be used in a wide variety of measurements that require frequency sweeping. A given number of points are measured within the user specified frequency range, or a manual list of measurement frequencies can be given. A linear or exponential sweeping can be selected, the latter being often more rational when large frequency range is used. Measurements are done by using either the lock-in amplifier or the multimeter. When high accuracy is required, also the frequency response of the signal generator should be measured for comparison.

Most accurate AC measurements can be done with the multimeter using a so called synchronous sub-sampled computed true RMS technique. It provides excellent linearity and a frequency range of 1 Hz to MHz. However, the method required the input signal to be repetitive, so measurements using changing frequency or noise are impossible. At frequencies below 1 kHz the accuracy is typically around 0,01 percent. The VI *Multimeter sub-sampled* was written to simplify the usage of the method. The VI takes a given number of measurements at a given precision target precision. It should be noted that the measurements at precision are very time-consuming. More details about the measurement technique can be found in [59].

4.3 Programs for optical measurements

Typically a measurement setup requires rather customized measurements procedure. Therefore, measurement programs were written only for the two most common

measurements, where either wavelength or chopping frequency is controlled. More complicated measurements can easily be built with LabVIEW using the building blocks mentioned above.

Spectral measurement VI controls the monochromator and the filter wheel to take measurements with the lock-in amplifier at different wavelengths. The wavelength range and step increment are specified by user as well as all measurement related parameters. By default, a suitable filter is selected automatically, but manual selection is also possible. This is useful for example when testing or calibrating devices. *Frequency measurement* VI is very similar to electrical measurement *Frequency response* VI, except it controls the optical chopper instead the signal generator. *Combined measurement* VI combines these two measurements, so that both the wavelength and the chopping frequency are varied.

5 Lock-in amplifier linearity

There are not that many linearity measurements of a lock-in amplifier reported. Even though signals are processed digitally in modern lock-in amplifiers, they still require analog amplification, filtering and signal generation. These analog components are the main cause of nonlinearities in the amplifier. For many devices the linearity factor can change more than 0,1 % over a factor of two change in the output. However, the nonlinearity characteristics are found to be independent of the used reference frequency and time constants. [60]

Comparison measurements done between different amplifiers suggest that the linearity characteristics vary from one instrument to another [60]. When signals of very different magnitude are measured, the sensitivity of the lock-in amplifier has to be changed between measurements. This automatically changes the gain of the device's preamplifier. During the measurements it was found that this has a similar effect to the linearity characteristics as for changing from lock-in amplifier to another.

Typical linearity measurements involve an optical setup where comparison is done between different lock-in amplifiers. However, in this thesis a different approach was developed. The measurements were done with purely electrically generated signals in order to minimize all other nonlinearity sources from the measurement. Unfortunately, very low signal levels are required, which makes this method somewhat complicated. Compared to DC voltage, very low and precise AC voltage levels are hard to produce. Typical signal generators usually operate in volt and millivolt scale, yet measurements well below microvolt are often required in spectroscopy. In order to solve the problem, a precision attenuator was built. Its specifications and performance are explained in the first subchapter, the actual measurement setup is introduced in the second and the results of the linearity measurements are shown in the third.

5.1 Precision attenuator

In order to produce very small AC signals a precision attenuator was designed and built. This allows a signal generator to be used at constant signal level when the performance of the lock-in amplifier is measured at different voltage levels and frequencies. The attenuator was left as a part of the setup, since it provides a handy tool for calibrations.

5.1.1 Design

Because the attenuator is only used with low frequency signals, a straightforward method of attenuation based on resistance dividers was considered as the most suitable. The schematic of the device is presented in figure 5.1. The resistor network construction guarantees that the minor contact resistance of the rotary switch has virtually no effect to the attenuation. The circuit provides attenuations in decades from 1 to 10^{-5}, while the input resistance of the device is deliberately constant 200 kΩ at all attenuations.

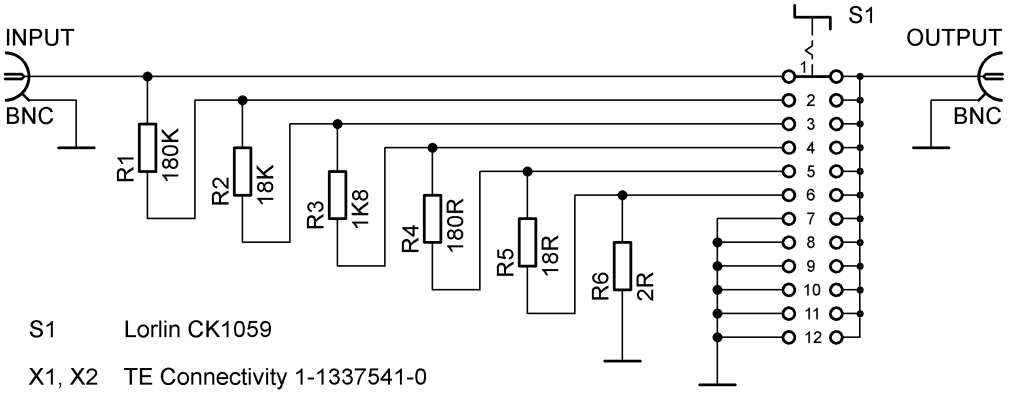

Figure 5.1 Schematic of the precision attenuator.

The right selection of resistors was the main issue in the design. In order to minimize the stray capacitances and impedances, 3.2 × 1.6 mm surface mount resistors were used. For values between 18 Ω to 180 kΩ high performance metal film resistors were used, but for the smallest 2 Ω resistance only thick film resistors were available. The key parameters of these components are shown in table 5.1.

Table 5.1 List of resistors used in the attenuator. [61], [62], [63]

No.	Tech.	Mfr.	Part number	Value	Toler.	Temp. coeff.
R1	Thin film	Panasonic	ERA8AEB184V	180 kΩ	±0,1 %	±25 ppm/°C
R2	Thin film	Panasonic	ERA8AEB183V	18 kΩ	±0,1 %	±25 ppm/°C
R3	Thin film	Panasonic	ERA8AEB182V	1,8 kΩ	±0,1 %	±25 ppm/°C
R4	Thin film	Panasonic	ERA8AEB181V	180 Ω	±0,1 %	±25 ppm/°C
R5	Thin film	Koa Speer	RN73H2BTTD18R0B25	18 Ω	±0,1 %	±25 ppm/°C
R6	Thick film	Vishay	CRCW12062R00FNEA	2 Ω	±1 %	±100 ppm/°C

Figure 5.2 illustrates the model for attenuator connection. All signal sources have nonzero output impedance Z_{out}. In signal generators the practice is to use 50 Ω or 75 Ω resistances in the output to match the impedance of coaxial cables. This causes a small voltage drop when the generator is loaded with the 200 kΩ input impedance of the attenuator that has to be taken into account. The first position in the attenuator's rotary switch only loads the signal source, but does not attenuate the output, so the actual voltage over the attenuator V_{in} can be measured and used as a reference value.

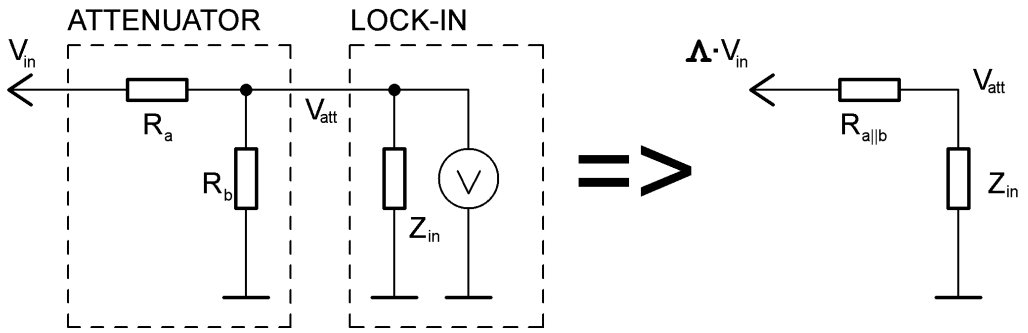

Figure 5.2 Model for attenuator connection. The voltage over the attenuator V_{in} can be measured using the first position of the attenuator.

Also the input impedance of the measurement device connected to the attenuator causes an error to actual attenuated voltage V_{att}. According to Thévenin's theorem, a resistive attenuator is equivalent to a single voltage source and a single series resistor. Figure 5.2 illustrates the principle. Parameter Λ is the nominal attenuation

$$\Lambda = \frac{R_b}{R_a + R_b} \tag{5.1}$$

and the resistance $R_{a||b}$ is the parallel connection of R_a and R_b

$$R_{a||b} = \frac{R_a R_b}{R_a + R_b}\,. \tag{5.2}$$

The actual attenuated voltage V_{att} can now be determined

$$V_{att} = \Lambda V_{in} \frac{Z_{in}}{Z_{in} + R_{a||b}}\,. \tag{5.3}$$

The assembled attenuator is presented in Figure 5.3. The attenuator's enclosure is galvanically isolated from the signal ground. This allows separate grounding to be used for noise cancellation. That is done most conveniently by using a floating signal generator with a separate guard wire for case grounding.

Figure 5.3 Precision attenuator assembled. The chassis ground marked GND and the signal ground are galvanically isolated.

5.1.2 Performance

The value R_b was measured using four-point measurement method for each attenuation setting. Keithley 263 calibrator was used as a current source and voltage was measured with Hewlett-Packard 3458A multimeter. The input resistance of the device was measured in the same way, which actually corresponds to value R_a+R_b. It was measured to be 199995,8 ± 1,1 Ω. From these values also the nominal attenuations Λ and parallel resistances $R_{a||b}$ were calculated. The results are shown in table 5.2.

Table 5.2 Measured resistances and calculated parameters of the attenuator. The uncertainty of the nominal attenuation is 400 ppm for the 10^{-5} setting and 150 ppm for the rest.

Setting	Resistance R_b [Ω]	Nominal attenuation Λ	parallel resistance $R_{a\|\|b}$ [Ω]
10^{-1}	20000,52 ± 0,1	1,0000E-01	18000,38 ± 0,2
10^{-2}	2000,213 ± 0,007	1,0001E-02	1980,208 ± 0,016
10^{-3}	200,0327 ± 0,0007	1,0002E-03	199,8326 ± 0,0016
10^{-4}	20,01394 ± 0,00007	1,0007E-04	20,01194 ± 0,00016
10^{-5}	2,000625 ± 0,000023	1,0003E-05	2,000605 ± 0,000040

Since AC signals are attenuated, the frequency response of the attenuator is also crucial. It was measured using Agilent 33521A as signal source. Measurements were done using the synchronous sub-sampled computed true RMS technique of the Hewlett-Packard 3458A multimeter. Linearity was determined by a comparison between attenuated and unattenuated signals in order to cancel out the nonlinearity of signal source. Frequencies up to 10 kHz were measured and the nonlinearities were less than 1 %. In the range of optical measurement frequencies, the attenuator performed better; the change in attenuation was less than 200 ppm up to 200 Hz with all attenuations.

5.2 Measurement setup

The measurement setup is shown in figure 5.4. The signal generator can produce signals in the RMS amplitude range of 1 mV to 1 V. The attenuator then allows the

measurements to be done in the range of 10 nV to 1 V. A separate BNC cable is used to provide the digital frequency reference to the lock-in amplifier. For comparison, signals in the range of 1 µV to 1 mV were measured with four different combinations of generator output and attenuation. The differences in results with different combinations were negligible.

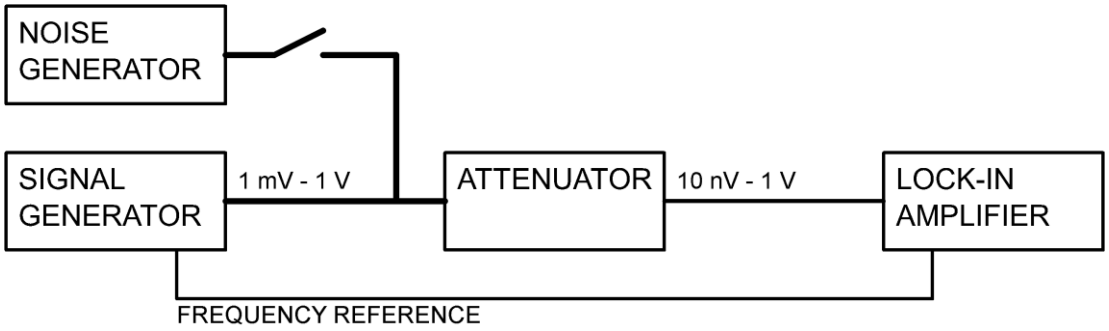

Figure 5.4 Measurement setup for electrical linearity and frequency response.

A noise generator was added to the measurement setup; both the noise and the signal generator have an output impedance of 50 Ω, so they were merely connected in series. The noise generator allows measurements below the single bit level of the lock-in amplifiers analog to digital converter (ADC). The noise causes a bit to change in the device and it can then be filtered as explained in section 2.6.1.

5.3 Linearity measurements

Linearity measurements were done within sensitivity ranges from 100 µV to 1 V. The sensitivity at the full range input voltage of a particular sensitivity ranges was used as a comparison value for relative sensitivity. For all ranges the nonlinearity was less than 1 % when the input voltage was more than 1 % of the full range voltage, and less than 2 % when the input voltage was more than 0,1 % of the full range voltage. Measuring signals below 1 % of the signal level is highly discouraged for the sheer problem of limited bits in the output value. As an example, the relative sensitivity of the lock-in

amplifier at 1 V range is shown in figure 5.5. For this range the measurements were also repeated by using the signal generator without the attenuator. The results for both measurements converge.

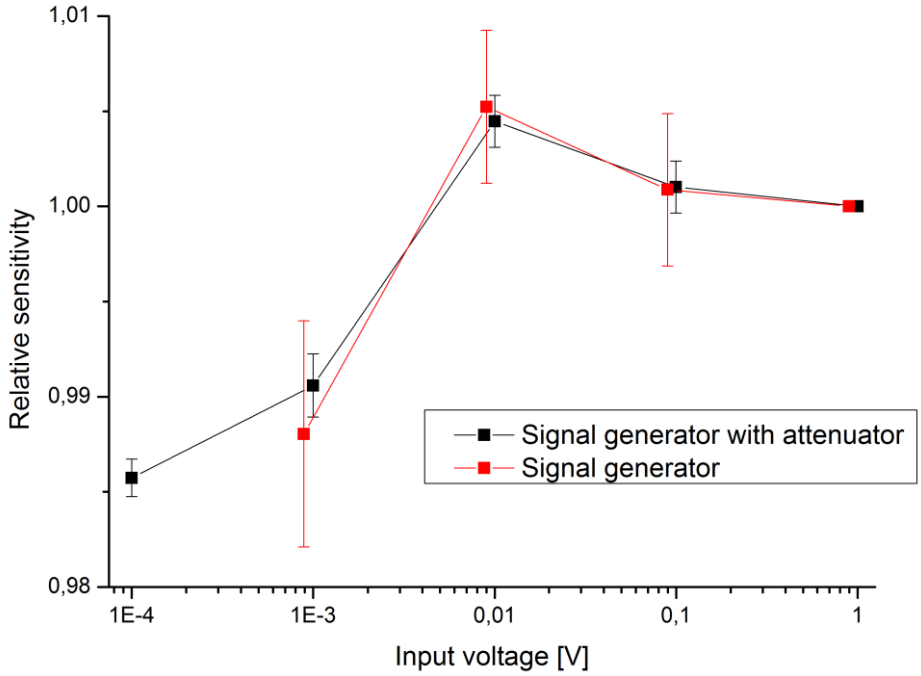

Figure 5.5 Relative sensitivity of the lock-in amplifier at 1 V range.

Also a comparison measurement between sensitivity ranges from 100 nV to 1 V was done. The sensitivity for every range was measured using 50 % of the full range voltage as the input voltage. These values were then scaled with the nominal sensitivity and compared to the 1 V sensitivity range. The determined values can be used as correction coefficients when different sensitivities are used in comparison measurements. The results are shown in figure 5.6.

An error of almost 15 % was measured in the 100 nV sensitivity range. This suspicious result was confirmed with two different signal generator signal levels using two different attenuations. The possibility of noise causing the measurement error was canceled out by repeating the two measurements with very long time constant of 30 s. Based on this result, one can conclude, that measurements using this sensitivity range

must be avoided. Fortunately omitting one sensitivity range is not a problem, because the measurements can be done with 1 µV sensitivity range as well.

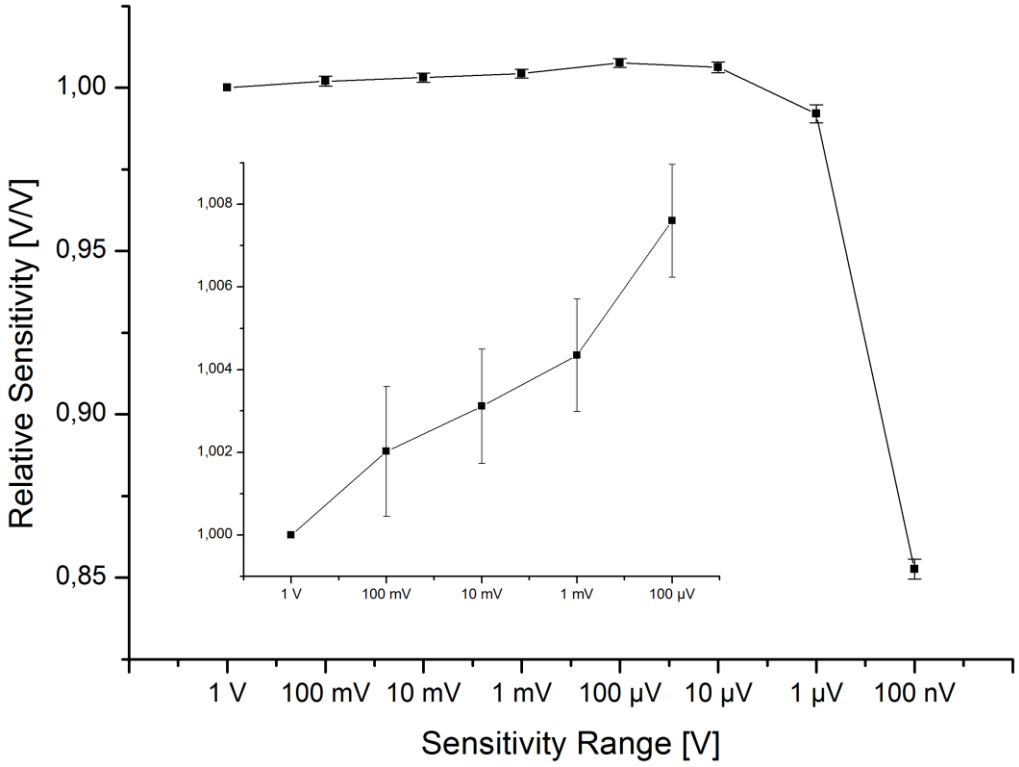

Figure 5.6 Comparison of sensitivity ranges. The sensitivities are scaled with nominal sensitivity of the range and compared to the value of the 1 V sensitivity range.

The test setup used for electrical linearity measurements was left to the spectrometer measurement setup. The linearity related uncertainty in comparison measurements is thus reduced from previous 0,35 % to 0,2 %, as correction coefficients for signals of different magnitude can easily be determined.

6 Preamplifier for photoconductive detectors

A preamplifier for photoconductive detectors was designed and built to replace a broken preamplifier. The old device was made according to the manufacturer's general recommendations for photodiode preamplifier. The design was mainly used with Hamamatsu Photonics P2038-03 lead selenide detector, albeit the gain, bias voltage and load resistance were optimized for MCT detectors and does not suit well for the specific detector [51]. Detailed schematics of the previous amplifier and along with explanatory text can be found in [3].

The design of the new amplifier is introduced in the first subchapter and the second focuses on the characterization of the device. Optical measurements done with the new amplifier are discussed in the third. Specifications of the amplifier are shown in table 6.1. The bandwidth of the amplifier is discussed more thoroughly in section 6.3.2.

Table 6.1 Specifications of the amplifier.

Gain	0, 20, 40 or 60 dB
Internal load resistance	1 kΩ - 32 MΩ, two values per decade
Input resistance	100 MΩ
Bandwidth	10 Hz - 200 Hz within 0,1 dB 1 Hz - 1,5 kHz within 3 dB
Internal biasing voltage	0 - 64 V
Internal biasing current	Max. 120 mA
External biasing voltage	Max. 400 V

6.1 Design

The new amplifier was designed so that it could be used with a wide variety of detectors. The old design served as a starting point for the new device and the basic amplifier topology is similar to the one demonstrated in [44]. The main feature of the new amplifier is the possibility to select gain, biasing voltage and load resistance, which

makes it a truly universal design. Complete schematics of the device and the list of components are in the appendices B and C, respectively.

The block diagram of the device is shown in figure 6.1. In addition to the actual preamplifier circuit, a biasing circuit is used to provide very stable biasing voltage through appropriate load resistance. Both the amplifier and the biasing circuit are controlled and monitored by the Arduino Uno microprocessor and front panel circuitry. The microcontroller is also used to control the front panel LCD. The complete program code along with comment text is listed in appendix D.

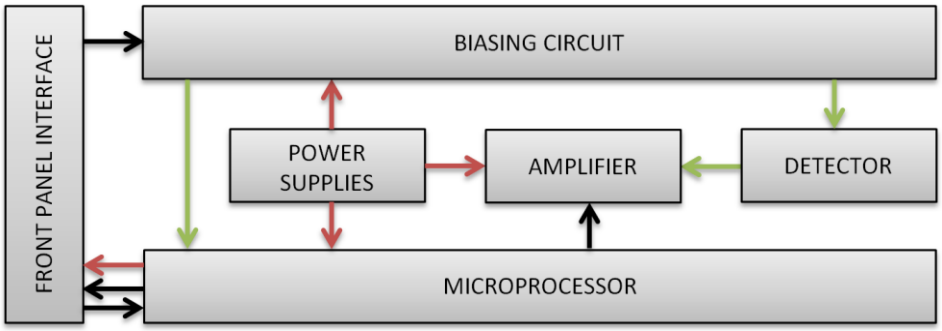

Figure 6.1 Block diagram of the preamplifier. Analog, digital and power signals are shown green, black and red, respectively.

6.1.1 Power supplies

Common linear regulators are used to maintain stable operating voltages of ±15 V. Input voltages for the regulators are provided from a single 15 VAC secondary coil using two parallel half-wave rectifiers in opposite polarity and reservoir capacitors. Third linear regulator is used to decrease the +15 V operating voltage to +9 V for the microcontroller. The microcontroller's own regulator is used to provide the +5 V logic voltages. However, a separate +5 V precision voltage reference is used with the microcontroller's ADC.

Two 25 VAC and one 15 VAC secondary coils are used in series to obtain a 65 VAC voltage. This is then rectified to a DC voltage of approximately +90 V. A high voltage regulator is then used to regulate a stable +75 V voltage for the biasing circuit. A

polymeric positive temperature coefficient device (PPTC) is placed before the regulator to limit the maximum current of the high voltage supply to around 120 mA. Toroidal transformers are used in the power supply to minimize electromagnetic interference, while a suppression filter is used to prevent radio frequency interference from the power grid.

6.1.2 Biasing circuit

A multi-turn potentiometer is used to adjust the biasing voltage. A 0 to 5 V setpoint voltage from the potentiometer is amplified with a high voltage operational amplifier to correspond to 0 to 64 V in the biasing output. NPN and PNP power transistors are used as a common-collector amplifier in front of the operational amplifier to boost the output current. The setpoint voltage is also measured with the microcontroller's ADC and the biasing voltage is displayed in the front panel LCD.

The front panel switch allows the user to select internal or external biasing voltage, or to use the amplifier without biasing at all. A rotary switch and a resistor network are used to select the load resistance. There are two built-in resistor values per decade, ranging from 1 kΩ to 32 MΩ. The last position of the rotary switch short-circuits internal load resistance network, enabling an arbitrary value external component to be used.

6.1.3 Amplifier circuit

A very simplified model of the amplifier circuit is shown in figure 6.2. Among other things, the model omits high pass filtering, overvoltage protection and gain selection implemented in the actual device.

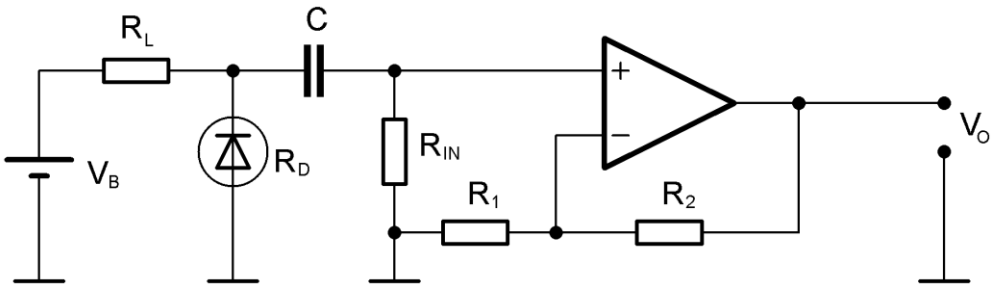

Figure 6.2 Simplified model of the amplifier circuit.

A large input resistance R_{IN} is used to keep the DC-component of the amplifier circuit zero. The low pass cut-off frequency f_c is determined by the R_{IN} and the filter capacitor C:

$$f_c = \frac{1}{2\pi R_{IN} C}. \tag{6.1}$$

The gain G is determined by the resistors R_1 and R_2:

$$G = 1 + \frac{R_2}{R_1}. \tag{6.2}$$

In the preamplifier the resistors R_1 and R_2 are replaced with a high precision integrated thin film network. A multiplexer controlled by the microcontroller is then used to change the feedback circuitry when gain is changed.

6.2 Characterization

Agilent 33521A signal generator was used with the attenuator introduced in chapter 5.1 as a signal source in the characterization measurements. Output voltages were measured with a Hewlett-Packard 3458A multimeter using the synchronous sub-sampled computed true RMS technique.

6.2.1 Gain

The gain of the amplifier was determined by comparing the input voltage from the signal generator and the output voltage from the preamplifier. Table 6.2 shows the measurement results. The difference between the nominal and measured gain is most likely due to the accuracy of the resistor network, with is 0,1 % for each separate resistor element. However, much more important factors are the high stability and low temperature coefficient of the divider network. The ratio between the decade dividing resistor, and thus the gain of the device, changes less than 50 ppm per year and the difference in temperature coefficients between two resistors is less than 2,5 ppm/°C [64].

Table 6.2 Measured gains of the preamplifier measured at 80 Hz.

Nominal gain	Input voltage [mV]	Output voltage [V]	Measured gain	Relative expanded uncertainty of measured gain [%] (*k* = 2)
0 dB	1001,471	1,000937	0,99947	0,015
20 dB	100,1426	0,998642	9,9722	0,03
40 dB	9,99342	0,99885	99,951	0,09
60 dB	0,99936	0,99754	998,17	0,1

6.2.2 Linearity

Linearity of the amplifier was measured by keeping the amplitude of the signal generator constant and measuring the output voltage at different attenuations. The results are shown in figure 6.3. At all nominal gains, smaller input voltage resulted in smaller measured gain.

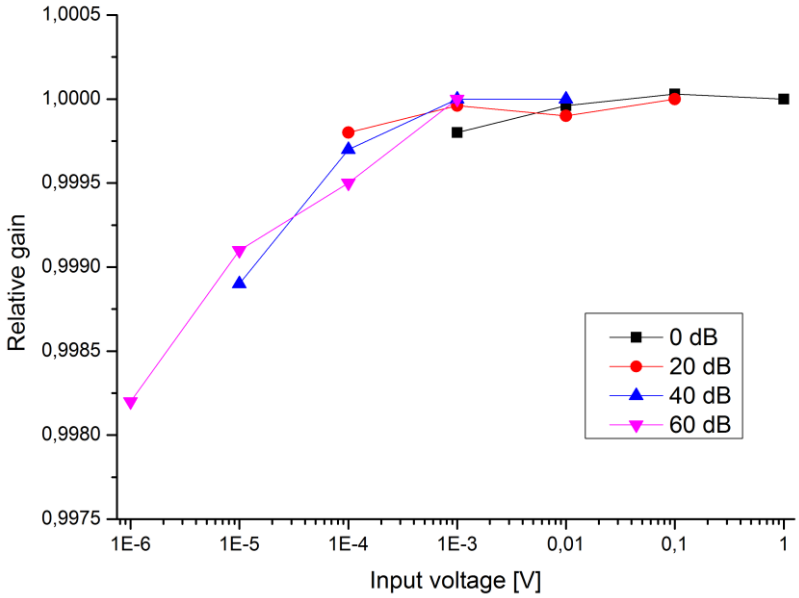

Figure 6.3 Linearity of the preamplifier measured at 80 Hz. Values are normalized with the value at 1V, 100 mV, 10 mV and 1 mV at gains 0, 20, 40 and 60 dB, respectively.

6.2.3 Frequency response

Low frequency response in the range of 10 to 200 Hz is shown in figure 6.4. This is the most interesting range, since it is important in optical measurements. In this range the three smallest gains have an very flat response and even the highest gain is flat within 0,1 dB.

Also the high frequency response was measured up to 10 kHz and is shown in figure 6.5. Due to the constant feedback capacitance of the amplifier circuit and the changing feedback resistance, the cutoff frequency lowers when gain is increased. But even with the highest gain the 6 dB cutoff frequency is around 6 kHz.

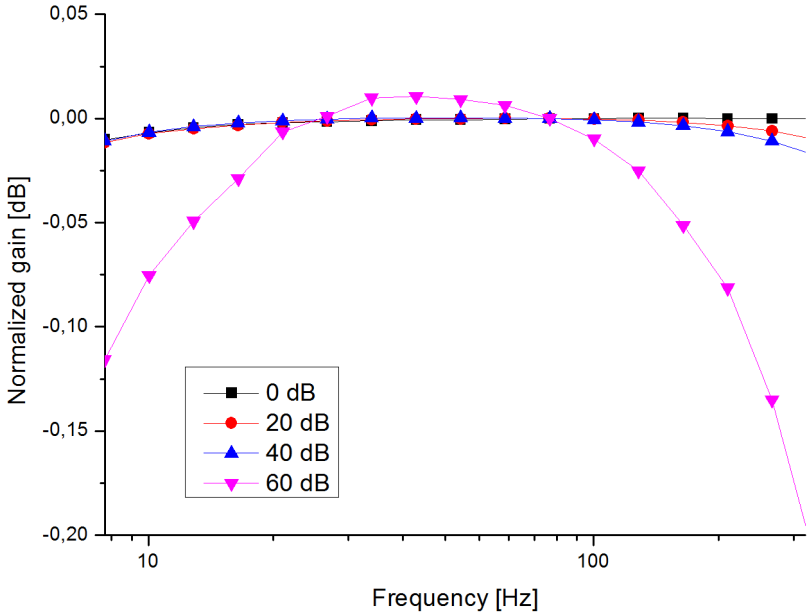

Figure 6.4 Frequency response of the preamplifier in the range of 10 to 200 Hz. Values are normalized with gain at 75 Hz frequency.

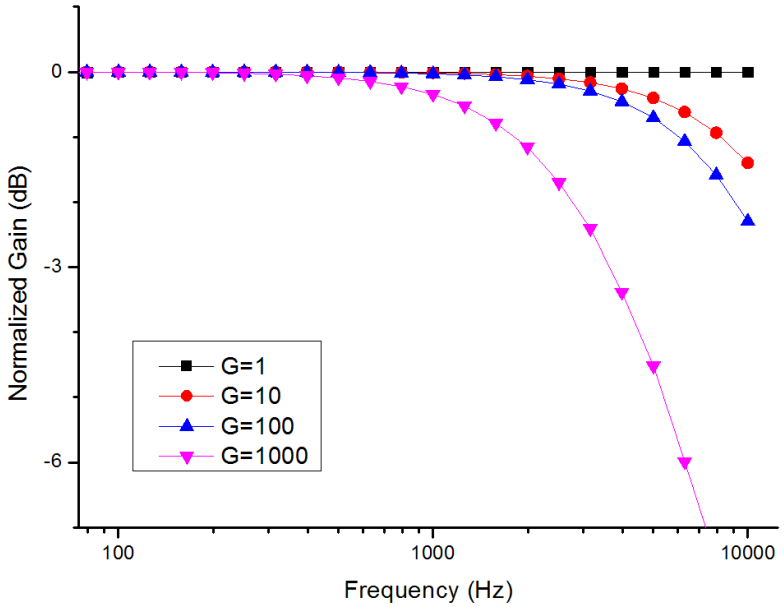

Figure 6.5 Frequency response of the preamplifier in the range of 100 Hz to 10 kHz. Values are normalized with gain at 100 Hz frequency.

6.3 Optical measurements

For comparison, optical measurements were done with Hamamatsu Photonics P2038-03 lead selenide detector with which the previous preamplifier was also used. With nominal biasing voltage of 50 V and with well-matched load resistance the responsivity of the detector increased approximately by a factor of 5 as compared to the values measured with the old preamplifier. The new amplifier also provides over 40 dB larger gain if needed, which improves the measurement of small signals.

According to the manufacturer's specifications, the responsivity of the P2038 -series detector is linear up to an incident energy level of around 1 mW/cm^2, after which it starts to decrease approximately by a factor of five per decade [51]. This behavior was confirmed, when the responsivity of the detector was measured with laser at power levels of 10 µW to 1 mW. Absolute values were obtained by comparison measurement with the pyroelectric reference detector. The results are shown in figure 6.5.

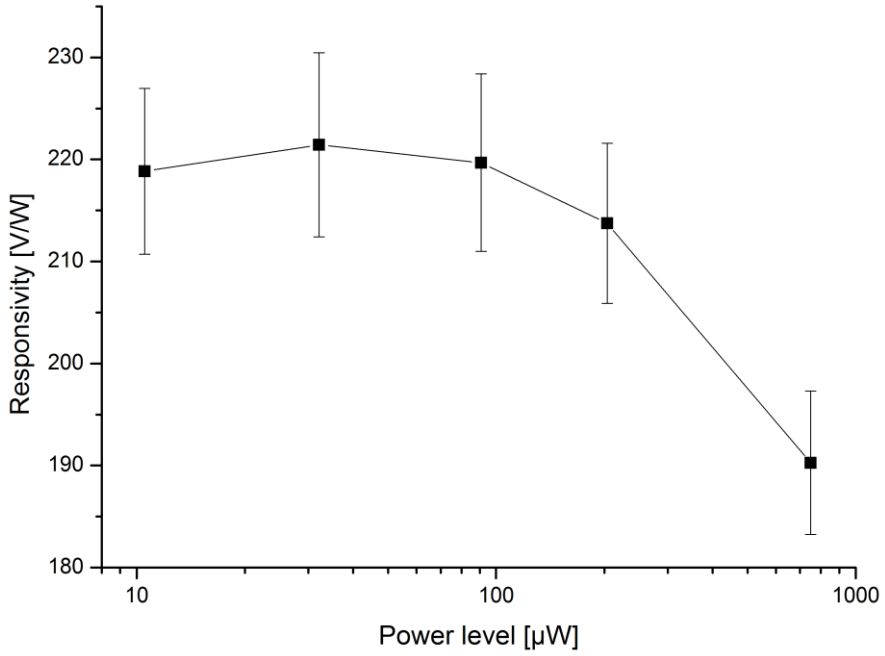

Figure 6.5 Responsivity of the PbSe photoconductive detector measured with 1,523 µm laser at 15 Hz chopping frequency. The detector was kept at a temperature just above 0 °C and a bias voltage of 30 V and a load resistance of 320 kΩ were used.

7 Conclusions

The fundamentals of optical radiometry and the theory of infrared sourcing, filtering and detection were considered. The current state of infrared radiation sources and detectors was reviewed. Furthermore, two amplification methods, phase sensitive detection and amplification of photoconductive detectors using load resistance for voltage extraction, were studied.

A facility for infrared measurements was extensively improved. The whole setup was refurbished and measurement and control devices were mounted to a rack to enhance and simplify the usability of the setup. The stability of the infrared sourcing and the quality of the measured signal from the reference detector were greatly enhanced. Also the previously uncharted low frequency response of the reference detector was determined. In addition, the improved facility enables a larger repertoire of infrared sources to be used.

The upgraded infrared spectrometer measurement setup is capable of measuring spectral responsivity of detectors, spectral transmittance of optical materials and spectral power distribution of light sources. Infrared detectors can be calibrated using the available solid-state detectors as working standards in the wavelength range of 1 to 5,1 µm and the pyroelectric reference detector in wavelength range of 750 nm to 16 µm. The expanded uncertainty of spectral responsivity calibrations is less than 3,7 %.

The automation software of the spectrometer measurement setup was fully updated. Virtually all measurement and control devices are now computer-controlled. Many aspects relating to computing and signal processing, for example the compensation for the nonlinearity in the monochromator's wavelength scale, was optimized. The most essential measurement and calibration programs were written. In addition, the versatile facility provides a user-friendly selection of tools for a wide variety of other measurement procedures.

The linearity of phase sensitive detection devices is not well known. The problem was studied in order to gain better understanding of nonlinearities in lock-in amplifier

measurements. As a result, a fully electrical method for linearity measurements of lock-in amplifiers was developed and tested. This method improves the accuracy in lock-in comparison methods and for example the nonlinearity component in the uncertainty of responsivity measurements is reduced to 0,2 %. The method can also be utilized for characterization of other amplifiers.

The amplification of a photoconductive detector's signal requires various parameters of the amplifier to be matched to the detector in question. Commonly a preamplifier is dedicated to some type of detectors. As a part of the thesis, a universal preamplifier for photoconductive detectors was designed, built, characterized and tested. It allows a single device to be used with a large variety of detectors. The preamplifier was also used in measurements to confirm the decrease in the response of lead selenide detectors at high power levels.

References

[1] Mohr P. J., Taylor B. N., Newell D. B., *The 2010 CODATA Recommended Values of the Fundamental Physical Constants, Web Version 6.0*, National Institute of Standards and Technology, 2011. [Referred: 19.11.2011]. Internet: http://physics.nist.gov/constants.

[2] Dereniak, E. L., Boreman, G. D., *Infrared Detectors and Systems*, New York, Wiley, 1996. 592 pp. ISBN 978-0471122098.

[3] Lano J., *Facility for Spectral Responsivity Measurements of Infrared Detectors*, Master's Thesis, HUT, Department of Electrical and Communications Engineering, Espoo, 2006. 54 pp.

[4] Valkonen M., *Development of Dry Nitrogen Purged Spectrometer for Infrared Region*, Master's Thesis, HUT, Department of Electrical and Communications Engineering, Espoo, 2007. 64 pp.

[5] Ahonen P., *Extension of Spectral Responsivity Scale for Infrared Detectors*, Master's Thesis, HUT, Department of Electrical and Communications Engineering, Espoo, 2009. 92 pp.

[6] Phillips A. C., *Introduction to Quantum Mechanics*. Chichester, John Wiley & Sons Ltd, 2003. 282 pp. ISBN 0-470-85323-9.

[7] Settle F. A., *Handbook of Instrumental Techniques for Analytical Chemistry*, Englewood Cliffs, New Jersey, Prentice-Hall, 1997. 995 pp. ISBN 978-0131773387.

[8] Parr A.C., Datla R.U., Gardner J.L., *Experimental Methods in the Physical Sciences: Vol 41. Optical Radiometry*, Amsterdam, Elsevier / Academic Press, 2005. 565 pp. ISBN 978-0124759886.

[9] Nash, M., *An investigation into the photocatalytic properties of microporous titanosilicate materials*, Doctoral Thesis, University of Delaware, Department of Chemical Engineering, Neward, 2008. 231 pp.

[10] Malacara D., Thompson B. J., *Handbook of Optical Engineering*, New York, Marcel Dekker Inc., 2001. 978 pp. ISBN 978-0-8247-9960-1.

[11] Pedrotti F. L., Pedrotti L. S., Pedrotti L. M., *Introduction to Optics,3rd edition*, New Jersey, Pearson Prentice Hall, 2007. 622 pp. ISBN 978-0131499331.

[12] Kingston R. H., *Optical Sources, Detectors, and Systems*, San Diego, Academic Press, 1995. 198 pp. ISBN 978-0124086555.

[13] Wolfe W. L, Zissis G. J., *The Infrared Handbook, 4th printing of revised edition*, Michigan, Environmental Research Institute of Michigan, 1993. 1700 pp. ISBN 0-9603590-1-X

[14] Shumaker D. L., Accetta J. S., *The Infrared and Electro Optical Systems Handbook*, Bellingham, SPIE Optical Engineering Press, 1993. 3524 pp. ISBN 978-0819410726

[15] Jones R. W., *Infrared Technology*. Kirk-Othmer Encyclopedia of Chemical Technology, 2000. [Referred: 2.11.2011]. Internet: http://onlinelibrary.wiley.com/doi/10.1002/0471238961.0914061810151405.a01/full

[16] Ballico M., *A simple technique for measuring the infrared emissivity of black-body radiators*, Metrologia, 2000. Vol. 37. Pp. 295-300. ISSN 1681-7575.

[17] Hecht E., *Optics, 4th edition*, San Fransisco, Addison Wesley, 2002, 698 pp. ISBN 0-321-18878-0.

[18] Product datasheet: *Incandescent reflector: infrared heat lamps/industrial*, Philips, 2002.

[19] Product datasheet: *Tungsten ribbon filament strip lamp,* The Pyrometer Instrument Company, Inc, 2008. [Referred 2.11.2011]. Internet: http://www.pyrometer.com/PDF_files/Optical%20Strip%20Lamp%2001-2008.pdf.

[20] Product datasheet: *IR-12 Series Miniature 8 to 11 Watt Infrared Emitter,* Boston Electronics Corporation, 2004. [Referred 2.11.2011]. Internet: http://www.boselec.com/documents/CWSourcesWWW5-3-05.pdf.

[21] Product datasheet: *Mini-Igniter^{TM} model 301,* Saint-Gobain Ceramics, 2007.

[22] Sperfeld P., Metzdorf J., Yousef Galal S., Stock K. D., Möller W., *Improvement and extension of the black-body-based spectral irradiance scale,* Metrologia, 1998. Vol. 35. Pp. 267-271. ISSN 1681-7575.

[23] Yousef Galal S., Sperfeld P., Metzdorf J., *Measurement and calculation of the emissivity of a high-temperature black body,* Metrologia, 2000. Vol 37. Pp. 365-368. ISSN 1681-7575.

[24] Yang R. Q., Lin C-H., Murry S J., Pei S. S., *Interband cascade light emitting diodes in the 5–8 μm spectrum region,* Applied Physics Letters, 1997. Vol. 70, Pp. 2013-1015. ISSN 0003-6951.

[25] Zibik E. A., Ng W. H., Revin D. G., Wilson L. R., Cockburn J. W., Groom, K. M., Hopkinson, M., *Broadband 6 μm<λ<8 μm superluminescent quantum cascade light-emitting diodes,* Applied Physics Letters, 2006. Vol. 88. 121109. ISSN 0003-6951.

[26] Jayaraman V., Strand T. A., Leonard D. B., Patent: *Multi-wavelength light source for spectroscopy,* US Patent No. 7880882 B2, 2011.

[27] Ng, W., Zibik E. A., Soulby M. R., Wilson L. R., Cockburn J. W., *Broadband quantum cascade laser emitting from 7.7 to 8.4 μm operating up to 340K,* Journal of Applied Physics, 2007. Vol. 101. 046103. ISSN 1089-7550.

[28] Kim J., Chen M., Yang C., Lee J., Yin S. S., Ruffin P., Edwards E., Brantley C., Luo C., *Broadband IR supercontinuum generation using single crystal sapphire fibers*, Optics Express, 2008. Vol. 16. Pp. 4085-4093. ISSN 1094-4087.

[29] Bridges J. M., Migdall A. L., *Characterization of argon arc source in the infrared*, Metrologia, 1995/96. Vol. 32. Pp. 625-628. ISSN 0026-1394.

[30] Schrama C. A., Bloembergen P., van der Ham E. W. M., *Monochromator-based cryogenic radiometry between 1 µm and 20 µm*, Metrologia, 2000. Vol. 37. Pp. 567-570. ISSN 0026-1394

[31] Product datasheet: *IR Mirrors*, Thorlabs, 2009. [Referred: 22.11.2011]. Internet: http://www.thorlabs.de/Navigation.cfm?Guide_ID=2143.

[32] Brown R. J. C., Brewer P. J., Milton M. J. T., *The physical and chemical properties of electroless nickel–phosphorus alloys and low reflectance nickel–phosphorus black surfaces*, Journal of Materials Chemistry, 2002. Vol. 12. Pp. 2749-2754. ISSN 1364-5501.

[33] Mizuno K., Ishii J., Kishida H., Hayamizu Y., Yasuda S., Futaba D. N., Yumura M., Hata K., *A black body absorber from vertically aligned single-walled carbon nanotubes*, Proceedings of the National Academy of Sciences of the United States of America, 2009. Vol. 106. 6044-7. ISSN 0027-8424.

[34] Product datasheet: *Optical Cast Infrared (IR) Longpass Filters*, Edmund Optics Ltd., 2011. [Referred 7.11.2011]. Internet: http://www.edmundoptics.com/products/displayproduct.cfm?productid=1918 .

[35] Product datasheet: *IR Long Pass Filters*, Wavelength technology Ltd., 2011. [Referred 7.11.2011]. Internet: http://www.wavelength-tech.com/IR-Optics/IRLongPassFilter.jsp.

[36] Donati S., *Photodetectors: Devices, Circuits and Applications*, New Jersey, Prentice Hall, 1999, 432 pp. ISBN 978-0130203373.

[37] Rogalski A., *Infrared detectors: an overview*, Infrared Physics & Technology, 2002. Vol 43. Pp. 187-210. ISSN 1350-4495.

[38] Rogalski A., *Infrared detectors: status and trends*, Progress in Quantum Electronics, 2003. Vol. 27. Pp. 59-210. ISSN 0079-6727.

[39] Guériaux V., de l'Isle N. B., Berurier A., Huet O., Manissadjian A., Facoetti H., Marcadet X., Carras M., Trinité V., Nedelcu A., *Quantum well infrared photodetectors: present and future*, Optical Engineering, 2011. Vol. 50. 061013. ISSN 0091-3286.

[40] Liu H. C., *Quantum dot infrared photodetector*, Opto-Electronics Review, 2003. Vol 11. Pp. 1-5. ISSN 1896-3757.

[41] Stanford Research Systems Inc., *Application Note #3: About Lock-In Amplifiers*, Stanford Research Systems Inc., 2004. [Referred: 11.11.2011]. Internet: http://www.thinksrs.com/downloads/PDFs/ApplicationNotes/AboutLIAs.pdf

[42] User Manual: *Model SR830 DSP Lock-In Amplifier, revision 6/2005,* Stanford Research Systems Inc., 2005.

[43] McNaught A. D., Wilkinson A., *IUPAC Compendium of Chemical Terminology, Second Edition,* Hoboken, New Jersey, Blackwell-Wiley, 1997. 464 pp. ISBN 978-0865426849.

[44] Hamamatsu Photonics K.K., *Technical Information SD-12: Characteristics and use of infrared detectors*, 2011. [Referred: 18.10.2011]. Internet: http://sales.hamamatsu.com/assets/applications/SSD/infrared_kird9001e04.pdf.

[45] User manual: *DC Power Supply HY3000 – HY5000 double series*, Precision Mastech Enterprises Co., 2006. [Referred: 16.11.2011]. Internet: http://hades.mech.northwestern.edu/images/f/f7/Mastech_power_supply_manual.pdf.

[46] User manual: *DC Power Supply AL 924A, revision 12/09*, elc, 2009.

[47] User manual: *МДР-23 Technical Description and Operating Instructions Ю-34.14.515 ТО*, 1988.

[48] Henricson J., *Monochromator controller*, Special assignment, Metrology laboratory, HUT, 2003. 22 pp.

[49] Manoochehri F., Kärhä P., Palva L., Toivanen P., Haapalinna A., Ikonen E., *Characterisation of optical detectors using high-accuracy instruments*, Analytica Chimica Acta, 1999. Vol. 380. Pp. 327-337. ISSN 0003-2670.

[50] Product datasheet: *SPH-40 Series: Hybrid Pyroelectric Detector*, Spectrum Detector Inc., 2010. [Referred: 17.11.2011]. Internet: http://www.crazyfingers.com/spectrum/pdf/datasheets/SPH-40.pdf.

[51] Product datasheet: *PbSe photoconductive detector P791/P2038/P2680 series, P3207-05*, Hamamatsu Photonics K.K., 2008. [Referred 2.11.2011]. Internet: http://sales.hamamatsu.com/assets/pdf/parts_P/p791-11_etc_kird1020e07.pdf.

[52] Product datasheet: *Lead Sulfide / Lead Seledine Detectors, J13 / J14 Series*, Judson Technologies LLC, 2002.

[53] User manual: *Series PS300 High Voltage Power Supplies*, Stanford Research System Inc., 2007. [Referred 23.11.2011]. Internet: http://www.thinksrs.com/downloads/PDFs/Manuals/PS300m.pdf.

[54] User manual: *Signal Recovery Model 3830 multiplexer*, Ametek Advanced Measurement Technology Inc., 2004.

[55] User manual: *HMI41 Indicator and HPM41/45/46 Probes, Vaisala, 1998.*

[56] Talvitie H., *Narrowing the spectral linewidth of a semiconductor laser*, Master's Thesis, HUT, Department of Electrical and Communications Engineering, Espoo, 1993. 48 pp.

[57] User manual: *IT116 flash / IT116 mini*, isel, 2009.

[58] User manual: *LabVIEW 2011*, National Instruments, 2011. [Referred: 16.1.2012]. Internet: http://www.ni.com/pdf/manuals/371361h.zip.

[59] User manual: *HP 3458A Multimeter edition 3*, Hewlett Packard, 1994.

[60] Theocharous E., *Absolute linearity characterization of lock-in amplifiers,* Applied Optics, 2008. Vol. 47. Pp. 1090-1096. ISSN 0003-6935.

[61] Product datasheet: *Metal Film (Thin Film) Chip Resistors, Type: ERA 2A, 3A, 6A, 8A*, Panasonic, 2011. [Referred 25.11.2011]. Internet: http://industrial.panasonic.com/www-data/pdf/AOA0000/AOA0000CE26.pdf.

[62] Product datasheet: *Surface Mount Resistors RN73H*, KOA Speer Electronics, 2011. [Referred: 25.11.2011]. Internet: http://www.koaspeer.com/products/resistors/surface-mount-resistors/rn73h/.

[63] Product datasheet: *Standard Thick Film Chip Resistors D/CRCW e3*, Vishay, 2011. [Referred: 25.11.2011]. Internet: http://www.vishay.com/docs/20035/dcrcwe3.pdf.

[64] Product datasheet: *CNS 471 Decade Divider Thin Film Resistor Networks*, Vishay, 2006. [Referred: 12.1.2012]. Internet: http://www.vishay.com/docs/60043/cns471st.pdf.

[65] Taylor B. N., Thompson A., *NIST Special publication 330, 2008 edition: The International System of Units (SI),* National Institute of Standards and Technology, 2008. [Referred: 31.10.2011]. Internet: http://physics.nist.gov/Pubs/SP330/sp330.pdf.

Appendices

Appendix A. Radiometric Quantities in SI units

Appendix B. Photoconductive detector preamplifier, schematics

Appendix C. Photoconductive detector preamplifier, list of components

Appendix D. Photoconductive detector preamplifier, program code

Appendix A. Radiometric Quantities in SI units

Table A1 presents radiometric quantities in SI units. It should be noted that a wide range of different symbols are commonly used in the literature. Spectral quantities can also be given per unit frequency, in which case they are commonly denoted with suffix υ.

Table A1. SI units in radiometry. [43], [65]

Quantity	**Symbol**	**Unit**	**Definition**
Radiant energy	Q_e	$J = kg \cdot m^{-2} \cdot s^{-2}$	The total energy emitted, transferred or received as radiation in a defined period of time
Radiant flux	Φ_e	$W = kg \cdot m^{-2} \cdot s^{-3}$	Power emitted, transferred or received as radiation
Spectral power	$\Phi_{e\lambda}$	$W \cdot m^{-1} = kg \cdot m^{-3} \cdot s^{-3}$	Radiant power per wavelength
Radiant intensity	I_e	$W \cdot sr^{-1} = kg \cdot m^{-2} \cdot s^{-3} \cdot sr^{-1}$	Radiant power per unit solid angle
Spectral radiant intensity	$I_{e\lambda}$	$W \cdot m^{-1} \cdot sr^{-1} = kg \cdot m^{-3} \cdot s^{-3} \cdot sr^{-1}$	Radiant intensity per wavelength
Radiance	L_e	$W \cdot m^{-2} \cdot sr^{-1} = kg \cdot m^{-4} \cdot s^{-3} \cdot sr^{-1}$	Radiant power per unit solid angle per unit projected source area.
Spectral radiance	$L_{e\lambda}$	$W \cdot m^{-3} \cdot sr^{-1} = kg \cdot m^{-5} \cdot s^{-3} \cdot sr^{-1}$	Radiance per wavelength
Irradiance	E_e	$W \cdot m^{-2} = kg \cdot m^{-4} \cdot s^{-3}$	Radiant power incident on a surface
Spectral irradiance	$E_{e\lambda}$	$W \cdot m^{-3} = kg \cdot m^{-5} \cdot s^{-3}$	Irradiance per wavelength
Radiant exitance or radiant emittance	M_e	$W \cdot m^{-2} = kg \cdot m^{-4} \cdot s^{-3}$	Power emitted per unit source

Appendix B. Photoconductive detector preamplifier, schematics

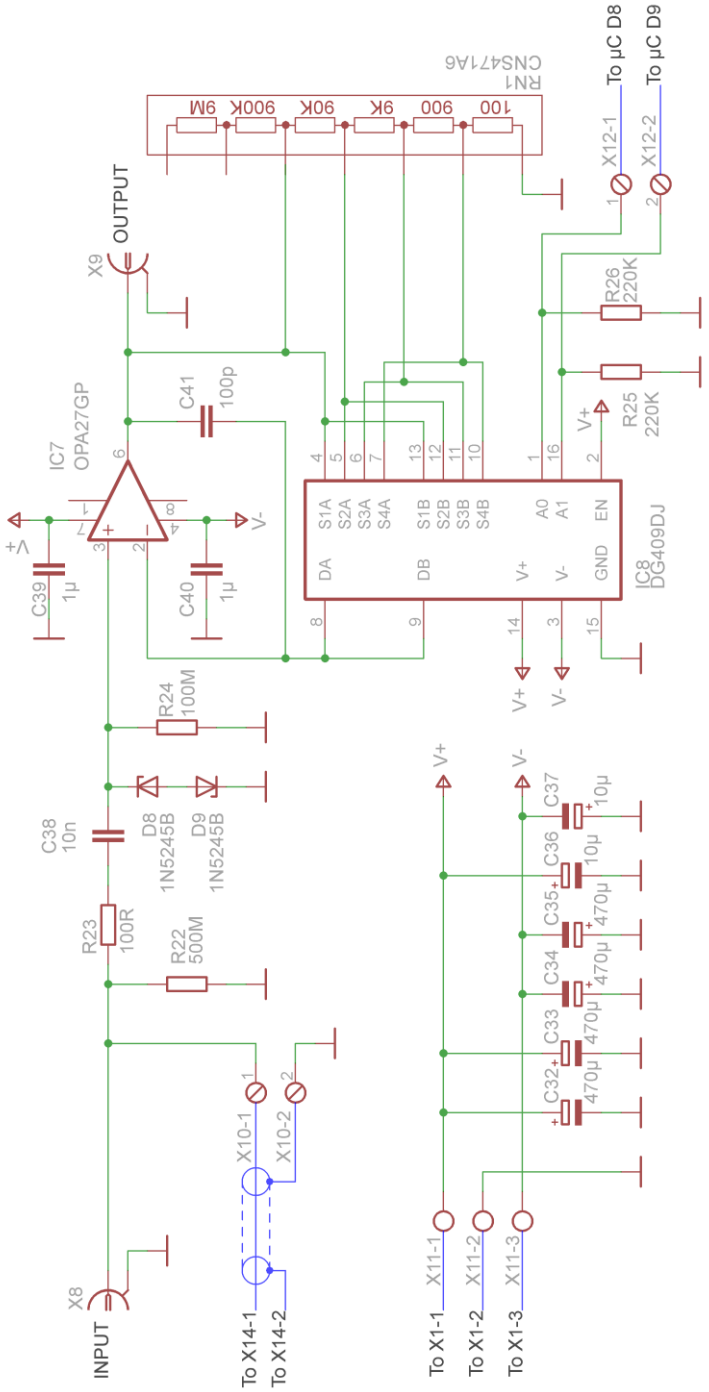

Figure B1. Schematic of the preamplifier circuit.

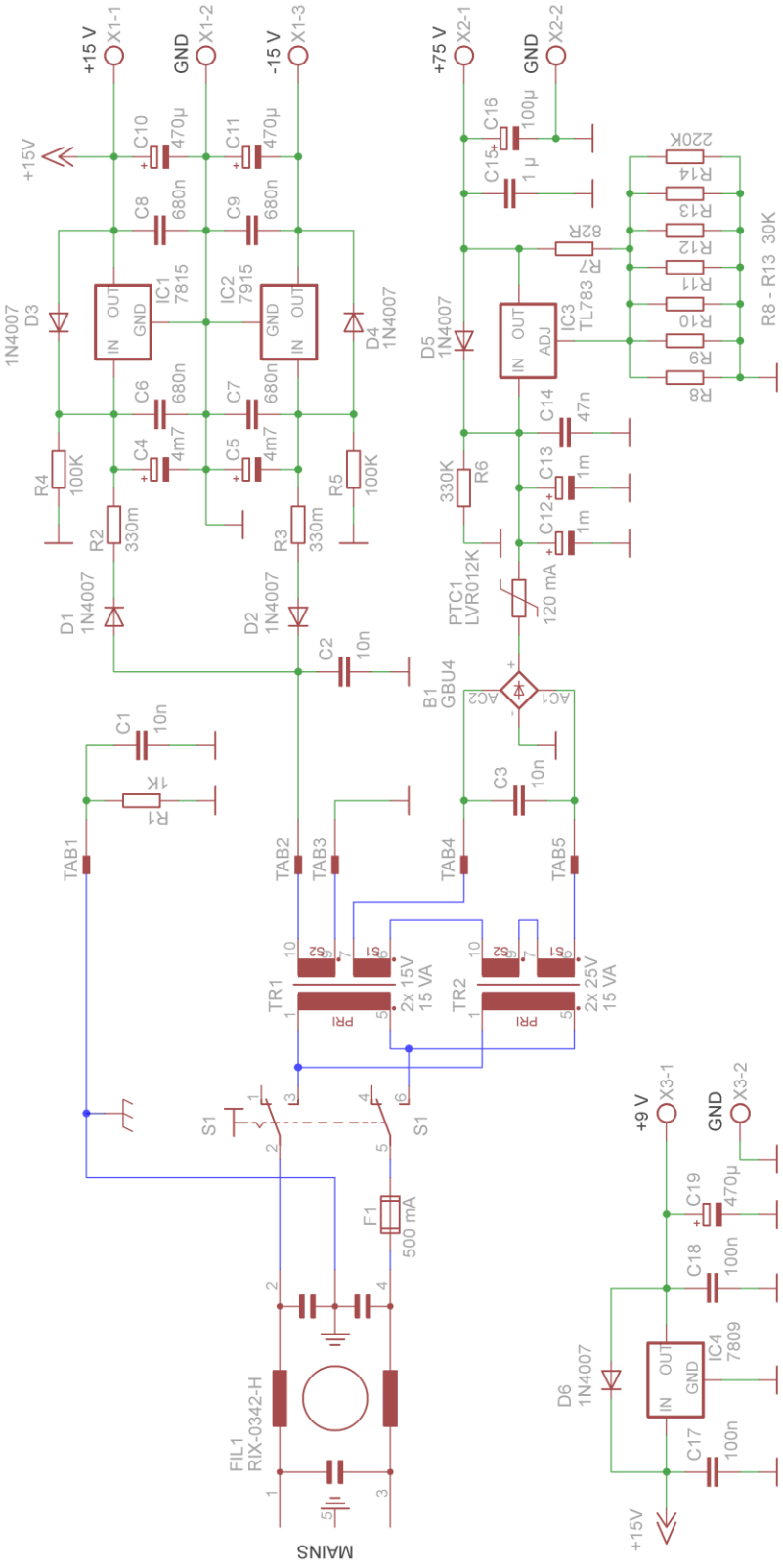

Figure B2. Schematic of the power supply and mains voltage wiring.

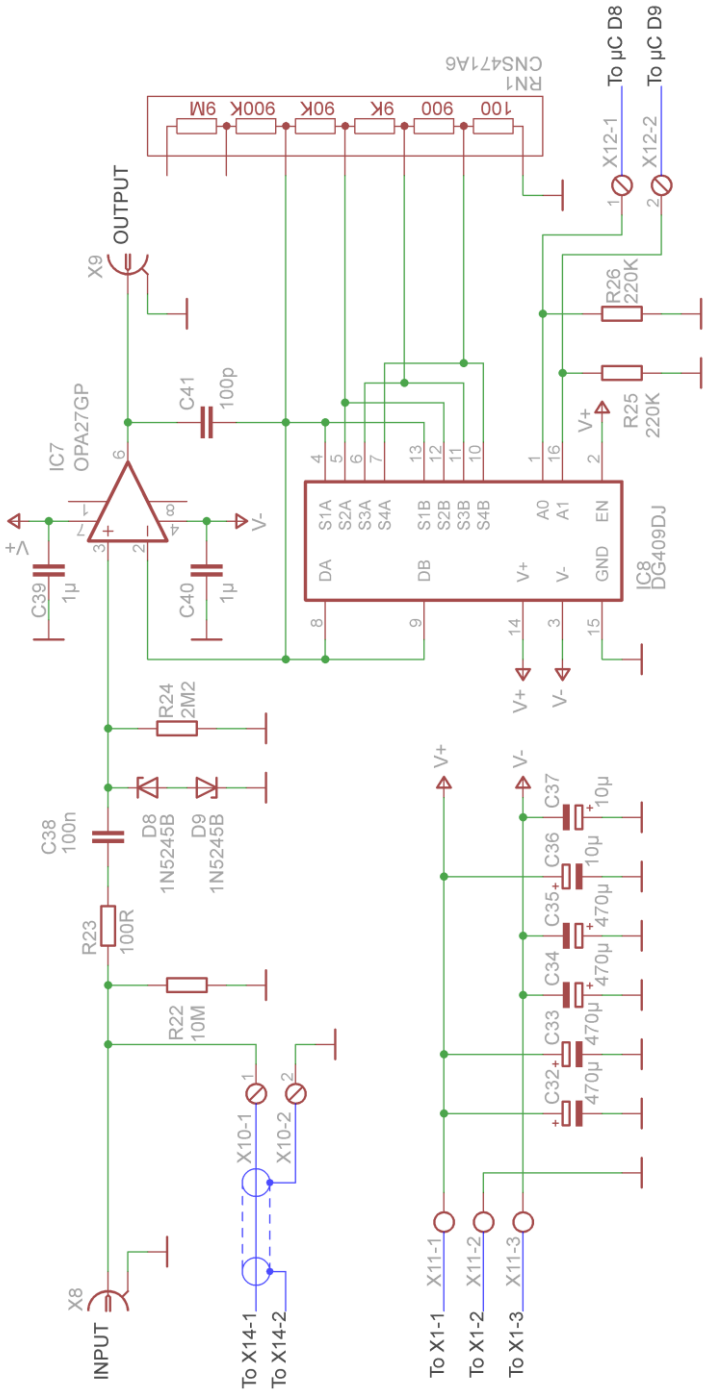

Figure B3. Schematic of the biasing circuit.

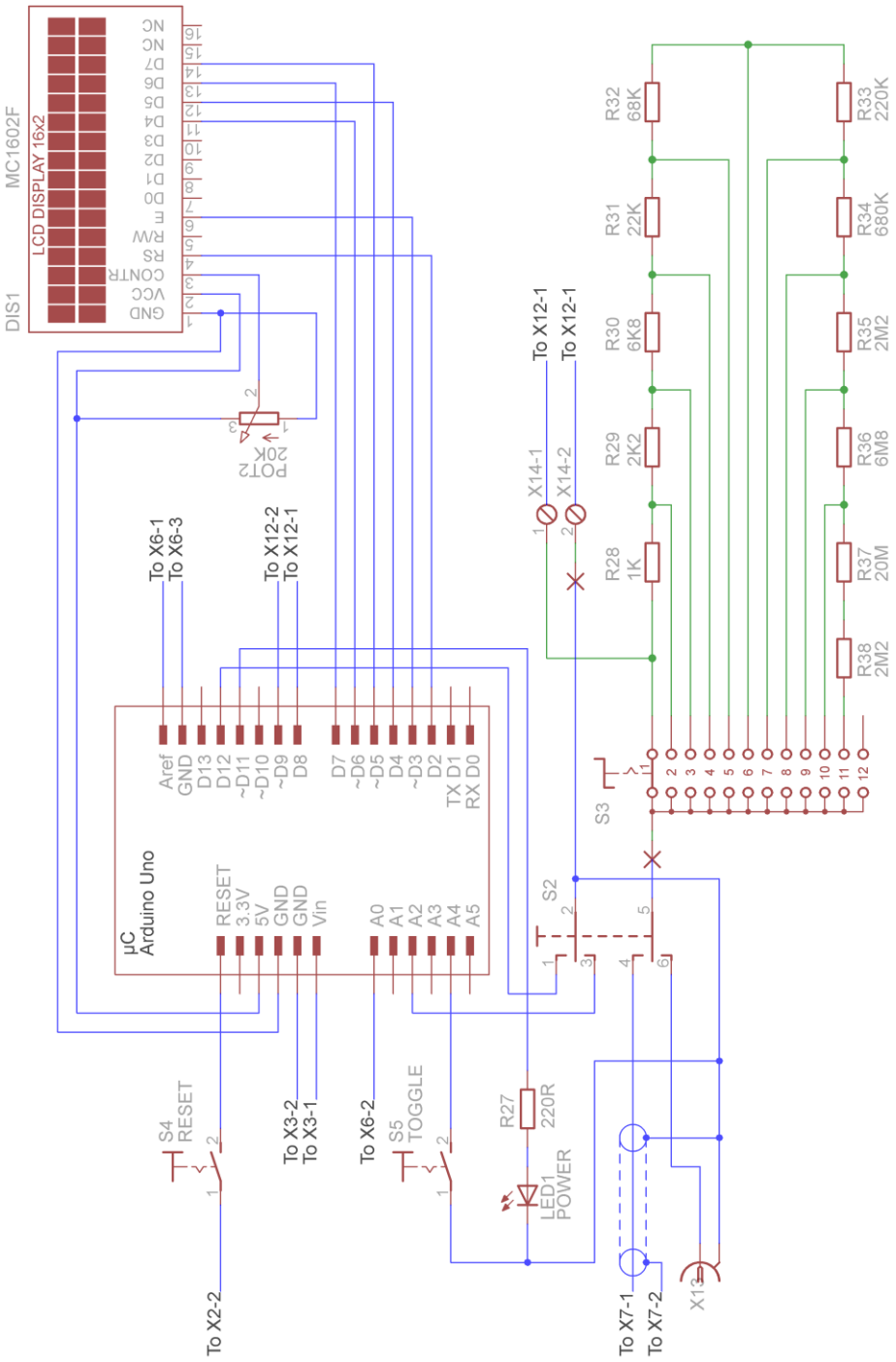

Figure B4. Schematic of the front panel circuitry and microcontroller wiring

Appendix C. Photoconductive detector amplifier, list of components

B1	Diode bridge	GBU4K	4 A	800 V		
C1	Capacitor, Polyester film	MMK5 103K400J01L4	10 nF	400 V	±10%	
C2	Capacitor, Polyester film	MMK5 103K400J01L4	10 nF	400 V	±10%	
C3	Capacitor, Polyester film	MMK5 103K400J01L4	10 nF	400 V	±10%	
C4	Capacitor, Aluminum electrolytic	ECOS1VP472BA	4700 µF	35 V	±20%	85 °C
C5	Capacitor, Aluminum electrolytic	ECOS1VP472BA	4700 µF	35 V	±20%	85 °C
C6	Capacitor, Polyester film	MKS0C026800C00KSSD	680 nF	63 V	±10%	
C7	Capacitor, Polyester film	MKS0C026800C00KSSD	680 nF	63 V	±10%	
C8	Capacitor, Polyester film	MKS0C026800C00KSSD	680 nF	63 V	±10%	
C9	Capacitor, Polyester film	MKS0C026800C00KSSD	680 nF	63 V	±10%	
C10	Capacitor, Aluminum electrolytic	RE3-25V471M	470 µF	25 V	±20%	85 °C
C11	Capacitor, Aluminum electrolytic	RE3-25V471M	470 µF	25 V	±20%	85 °C
C12	Capacitor, Aluminum electrolytic	EETED2D102CA	1000 µF	200 V	±20%	105 °C
C13	Capacitor, Aluminum electrolytic	EETED2D102CA	1000 µF	200 V	±20%	105 °C
C14	Capacitor, Polyester film	MMK10 473K400A01L4	47 nF	400 V	±10%	
C15	Capacitor, Polyester film	MMK15 105K100B04L4	1 µF	100 V	±10%	
C16	Capacitor, Aluminum electrolytic	MCGPR100V107M13X21	100 µF	100 V	±20%	85 °C
C17	Capacitor, Polyester film	MKS2D031001A00KSSD	100 nF	100 V	±10%	
C18	Capacitor, Polyester film	MKS2D031001A00KSSD	100 nF	100 V	±10%	
C19	Capacitor, Aluminum electrolytic	RE3-25V471M	470 µF	25 V	±20%	85 °C
C20	Capacitor, Aluminum electrolytic	RE3-25V471M	470 µF	25 V	±20%	85 °C
C21	Capacitor, Aluminum electrolytic	RE3-25V471M	470 µF	25 V	±20%	85 °C
C22	Capacitor, Tantalum electrolytic	CB1E106M2CCB	10 µF	25 V	±20%	
C23	Capacitor, Multilayer ceramic	B37984M5105K	1 µF	50 V	±10%	
C24	Capacitor, Multilayer ceramic	K104K15X7RF5TH5V	100 nF	50 V	±10%	
C25	Capacitor, Polyester film	MMK15 105K100B04L4	1 µF	100 V	±10%	
C26	Capacitor, Polyester film	MKS0C026800C00KSSD	680 nF	63 V	±10%	
C25	Capacitor, Polyester film	MMK15 105K100B04L4	1 µF	100 V	±10%	
C26	Capacitor, Polyester film	MKS0C026800C00KSSD	680 nF	63 V	±10%	
C27	Capacitor, Ceramic Disc	MCCHU7101J5	100 pF	50 V	±5%	
C28	Capacitor, Polyester film	MMK15 105K100B04L4	1 µF	100 V	±10%	
C29	Capacitor, Polyester film	MKS0C026800C00KSSD	680 nF	63 V	±10%	
C30	Capacitor, Aluminum electrolytic	MCGPR100V226M8X11	22 µF	100 V	±20%	85 °C
C31	Capacitor, Aluminum electrolytic	MCGPR100V107M13X21	100 µF	100 V	±20%	85 °C
C32	Capacitor, Aluminum electrolytic	RE3-25V471M	470 µF	25 V	±20%	85 °C
C33	Capacitor, Aluminum electrolytic	RE3-25V471M	470 µF	25 V	±20%	85 °C
C34	Capacitor, Aluminum electrolytic	RE3-25V471M	470 µF	25 V	±20%	85 °C
C35	Capacitor, Aluminum electrolytic	RE3-25V471M	470 µF	25 V	±20%	85 °C
C36	Capacitor, Tantalum electrolytic	CB1E106M2CCB	10 µF	25 V	±20%	
C37	Capacitor, Tantalum electrolytic	CB1E106M2CCB	10 µF	25 V	±20%	
C38	Capacitor, Polypropylene film	FKP1R021005D00KSSD	10 nF	1250 V	±10%	
C39	Capacitor, Multilayer ceramic	B37984M5105K	1 µF	50 V	±10%	
C40	Capacitor, Multilayer ceramic	B37984M5105K	1 µF	50 V	±10%	
C41	Capacitor, Ceramic Disc	MCCHU7101J5	100 pF	50 V	±5%	
D1	Diode, Standard rectifier	1N4007	1 A	1000 V		
D2	Diode, Standard rectifier	1N4007	1 A	1000 V		
D3	Diode, Standard rectifier	1N4007	1 A	1000 V		
D4	Diode, Standard rectifier	1N4007	1 A	1000 V		
D5	Diode, Standard rectifier	1N4007	1 A	1000 V		
D6	Diode, Standard rectifier	1N4007	1 A	1000 V		
D7	Diode, Fast recovery rectifier	MR858	3 A	800 V		

D8	Diode, Zener	1N5245B	15 V	500 mW	
D9	Diode, Zener	1N5245B	15 V	500 mW	
DIS1	LCD module	MC1602F-SYR	16 x 2 CH		
F1	Fuse, Slow blow		500 mA	5 x 20 mm	
FIL1	Filter, Power line suppression	RIX-0342-H	3 A	50 Hz	
IC1	Linear regulator	MC7815CT	+15 V	1 A	TO-220
IC2	Linear regulator	MC7915CT	-15 V	1 A	TO-220
IC3	Linear regulator	TL783CKCSE3	1.25-125 V	700 mA	TO-220
IC4	Linear regulator	MC7815CT	+9 V	1 A	TO-220
IC5	Voltage reference	REF02APG4	+5 V	0.2%	DIP8
IC6	Operational amplifier, High voltage	OPA445AP	±45V	70 kHz	DIP8
IC7	Operational amplifier, Low noise	OPA27GP	8 MHz		DIP8
IC8	Analog multiplexer	DG409DJZ	4 x 2 CH	40 Ω	DIP16
LED1	Light-emitting diode		5 mm	Blue	
PTC1	Resettable fuse	LVR012K	120 mA	240V	
POT1	Potentiometer, Precision	3590S-2-103L	10 K	10 turn	
POT2	Potentiometer	3310C-1-203L	20 K		
Q1	Transistor, Bipolar NPN	TIP31C	3 A	40 W	TO-220
Q2	Transistor, Bipolar PNP	TIP31C	3 A	40 W	TO-220
R1	Resistor, Metal film		1 kΩ	600 mW	±2%
R2	Resistor, Metal film, flameproof	SPRX1/2C	330 mΩ	500 mW	±5%
R3	Resistor, Metal film, flameproof	SPRX1/2C	330 mΩ	500 mW	±5%
R4	Resistor, Metal film		100 kΩ	600 mW	±2%
R5	Resistor, Metal film		100 kΩ	600 mW	±2%
R6	Resistor, Metal film		330 kΩ	600 mW	±2%
R7	Resistor, Metal film		82 Ω	600 mW	±2%
R8	Resistor, Carbon composition		30 kΩ	1 W	±5%
R9	Resistor, Carbon composition		30 kΩ	1 W	±5%
R10	Resistor, Carbon composition		30 kΩ	1 W	±5%
R11	Resistor, Carbon composition		30 kΩ	1 W	±5%
R12	Resistor, Carbon composition		30 kΩ	1 W	±5%
R13	Resistor, Carbon composition		30 kΩ	1 W	±5%
R14	Resistor, Metal film		220 kΩ	600 mW	±2%
R15	Resistor, Metal film		10 MΩ	600 mW	±2%
R16	Resistor, Metal film		10 kΩ	600 mW	±2%
R17	Resistor, Metal film		27 kΩ	600 mW	±1%
R18	Resistor, Metal film		330 kΩ	600 mW	±1%
R19	Resistor, Metal film		100 Ω	600 mW	±2%
R20	Resistor, Metal film		220 mΩ	600 mW	±5%
R21	Resistor, Metal film		220 mΩ	600 mW	±5%
R22	Resistor, Thick film	HTS00635006JPB17	500 MΩ	500 mW	±5%
R23	Resistor, Metal film		100 Ω	600 mW	±2%
R24	Resistor, Thick film	HTS00631006JPB17	100 MΩ	500 mW	±5%
R25	Resistor, Metal film		220 kΩ	600 mW	±2%
R26	Resistor, Metal film		220 kΩ	600 mW	±2%
R27	Resistor, Metal film		220 Ω	600 mW	±2%
R28	Resistor, Metal film		1 kΩ	600 mW	±1%
R29	Resistor, Metal film		2,2 kΩ	600 mW	±1%
R30	Resistor, Metal film		6,8 kΩ	600 mW	±1%
R31	Resistor, Metal film		22 kΩ	600 mW	±1%
R32	Resistor, Metal film		68 kΩ	600 mW	±1%
R33	Resistor, Metal film		220 kΩ	600 mW	±1%
R34	Resistor, Metal film		680 kΩ	600 mW	±1%
R35	Resistor, Metal film		2,2 MΩ	600 mW	±1%
R36	Resistor, Metal film		6,8 MΩ	600 mW	±1%
R37	Resistor, Metal film		20 MΩ	600 mW	±1%
R38	Resistor, Metal film		2,2 MΩ	600 mW	±1%
RN1	Resistor network, 6 decade divider	CNS471A6	0,1%	±25ppm/°C	SIL8
S1	Switch, Toggle ON-ON	RT 556	2 A	250 VAC	

S2	Switch, Toggle ON-OFF-ON	MS-500H	6 A	125 VAC	
S3	Switch, Rotary 1 x 12	CK1059	250 mA	300 VAC	
S4	Switch, Pushbutton SPST-NO	R13-24AL-05-BB	3A	125 VAC	
S5	Switch, Pushbutton SPST-NO	R13-24AL-05-BR	3A	125 VAC	
TAB1	Tab, Straight	726386-2	6,3 x 0,8 mm		
TAB2	Tab, Straight	726386-2	6,3 x 0,8 mm		
TAB3	Tab, Straight	726386-2	6,3 x 0,8 mm		
TAB4	Tab, Straight	726386-2	6,3 x 0,8 mm		
TAB5	Tab, Straight	726386-2	6,3 x 0,8 mm		
TR1	Transformer, Toroidal	MCFE015/15	2 x 15 V	15 VA	
TR2	Transformer, Toroidal	MCFE015/25	2 x 25 V	15 VA	
X1	Connector, Terminal block	MSB03005	13 A	250 V	
X2	Connector, Terminal block	MSB02005	13 A	250 V	
X3	Connector, Terminal block	MSB02005	13 A	250 V	
X4	Connector, Terminal block	MSB03005	13 A	250 V	
X5	Connector, Terminal block	MSB02005	13 A	250 V	
X6	Connector, Terminal block	MSB03004	12 A	150 V	
X7	Connector, Terminal block	MSB03005	13 A	250 V	
X8	Connector, BNC socket, PCB	1-1337543-0	50 Ω	1500 V	4 GHz
X9	Connector, BNC socket, PCB	1-1337543-0	50 Ω	1500 V	4 GHz
X10	Connector, Terminal block	MSB02004	12 A	150 V	
X11	Connector, Terminal block	MSB03005	13 A	250 V	
X12	Connector, Terminal block	MSB02004	12 A	150 V	
X13	Connector, BNC socket, bulkhead	1-1337452-0	50 Ω	1500 V	4 GHz
X14	Connector, Terminal block	MSB02004	12 A	150 V	
µC	Microcontroller	Arduino Uno			

Appendix D. Photoconductive detector amplifier, program code

```
#include <LiquidCrystal.h>

// Mapping pins
#define  BIAS_VOLTAGE  A0
#define  TOGGLE        A4
#define  EXT_BIAS      A2
#define  INT_BIAS      12
#define  POWER         11
#define  GAIN0         8
#define  GAIN1         9

// LCD related pins
#define  ENABLE         3
#define  RS             2
#define  DB4            6
#define  DB5            4
#define  DB6            7
#define  DB7            5

// Voltage calculation coefficient
#define GAIN_COEFF      159.84375

// Object for LCD
LiquidCrystal lcd(RS, ENABLE, DB4, DB5, DB6, DB7);

// byte that carries gain information. Gain bits are the two least
signicant bits of the byte.
byte gain = 0;

// Boolean value for the toggle buttons last value
boolean last_toggle = false;

void setup()
{
  // Setting inputs and outputs
  pinMode(BIAS_VOLTAGE, INPUT);
  pinMode(TOGGLE, INPUT);
  pinMode(EXT_BIAS, INPUT);
  pinMode(INT_BIAS, INPUT);
  pinMode(POWER, OUTPUT);
  pinMode(GAIN0, OUTPUT);
  pinMode(GAIN1, OUTPUT);

  // Lighting up the power LED
  digitalWrite(POWER, HIGH);

  // Setting pull-up resistors
  digitalWrite(TOGGLE, HIGH);
  digitalWrite(EXT_BIAS, HIGH);
  digitalWrite(INT_BIAS, HIGH);
```

```
  // Initializing LCD
  lcd.begin(16,2);

  // Setting ADC reference to external
  analogReference(EXTERNAL);


  // Printing start message to LCD
  for(int i = 0; i <= 15; i++) {
    lcd.setCursor(0,0);
    lcd.print("Powering up...");
    lcd.setCursor(i,1);
    lcd.print("*");
    delay(300);
  }
  lcd.clear();
}

void loop() {

  /* Checking the bias switch position,
   calculating bias voltage and
   updating LCD values               */

  // If using external bias
  if(digitalRead(EXT_BIAS) == LOW) {
    lcd.setCursor(0,0);
    lcd.print("Bias: External  ");
  }

  // If no bias at all
  else if(digitalRead(INT_BIAS) == HIGH) {
    lcd.setCursor(0,0);
    lcd.print("Bias: Off       ");
  }

  // If using internal bias
  else {

    // Reading bias voltage value by taking 10 samples to average out
the noise
    long bias_value = 0;

    for(int i = 0; i <= 9; i++) {
      bias_value += analogRead(BIAS_VOLTAGE);
    }

    // Averaging
    float print_value = (float)bias_value/GAIN_COEFF;

    // Rounding off the value
    print_value *= 10.0;
    print_value += 0.5;
    bias_value = (int)print_value;
    print_value = (float)bias_value/10.0;
```

```
    // Printing text
    lcd.setCursor(0,0);
    lcd.print("Bias:      Volts");


    // Moving cursor to right position depending on the number of
digits
    if(bias_value < 100) {
      lcd.setCursor(7,0);
    }
    else {
      lcd.setCursor(6,0);
    }

    // Printing the calculated value
    lcd.print(print_value);

    // Masking off an extra zero
    lcd.setCursor(10,0);
    lcd.print(" ");
  }


  /* Checking if changing the gain is
   needed and updating LCD values            */

  // If the toggle button is being pushed yet without toggle
operation?
  if(digitalRead(TOGGLE) == LOW && last_toggle == false) {

    // Wait for a moment and check again to avoid double contacts.
    delay(25);
    if(digitalRead(TOGGLE) == LOW) {
      last_toggle = true;
      gain += 1;
    }
  }

  // If not pressing, change last toggle to false
  if(digitalRead(TOGGLE) == HIGH) {

    // Wait for a moment and check again to double contacts.
    delay(25);
    if(digitalRead(TOGGLE) == HIGH) {
      last_toggle = false;
    }
  }

  // Changing gain if needed and updating the LCD
  lcd.setCursor(0,1);

  switch (gain % 4) {

  case 0:
    lcd.print("Gain: 1         ");

    if(digitalRead(GAIN0 == HIGH))
```

```
      digitalWrite(GAIN0, LOW);

    if(digitalRead(GAIN1 == HIGH))
      digitalWrite(GAIN1, LOW);

    break;

  case 1:
    lcd.print("Gain: 10        ");

    if(digitalRead(GAIN0 == LOW))
      digitalWrite(GAIN0, HIGH);

    if(digitalRead(GAIN1 == HIGH))
      digitalWrite(GAIN1, LOW);

    break;

  case 2:
    lcd.print("Gain: 100       ");

    if(digitalRead(GAIN0 == HIGH))
      digitalWrite(GAIN0, LOW);

    if(digitalRead(GAIN1 == LOW))
      digitalWrite(GAIN1, HIGH);

    break;

  case 3:
    lcd.print("Gain: 1000      ");

    if(digitalRead(GAIN0 == LOW))
      digitalWrite(GAIN1, HIGH);

    if(digitalRead(GAIN1 == LOW))
      digitalWrite(GAIN1, HIGH);

    break;

  default:
    lcd.print("Undefined gain! ");
  }

  delay(50);
}
```